

Guided by Stars: Interpretable Concept Learning Over Time Series via Temporal Logic Semantics

IRENE FERFOGLIA*, Università degli Studi di Trieste, Italy

SIMONE SILVETTI, Università degli Studi di Trieste, Italy

GAIA SAVERI, Università degli Studi di Trieste, Italy

LAURA NENZI, Università degli Studi di Trieste, Italy

LUCA BORTOLUSSI*, Università degli Studi di Trieste, Italy

Time series classification is a task of paramount importance, as this kind of data often arises in safety-critical applications. However, it is typically tackled with black-box deep learning methods, making it hard for humans to understand the rationale behind their output. To take on this challenge, we propose a novel approach, STELLE (Signal Temporal logic Embedding for Logically-grounded Learning and Explanation), a neuro-symbolic framework that unifies classification and explanation through direct embedding of trajectories into a space of temporal logic concepts. By introducing a novel STL-inspired kernel that maps raw time series to their alignment with predefined STL formulae, our model jointly optimises accuracy and interpretability, as each prediction is accompanied by the most relevant logical concepts that characterise it. This yields (i) local explanations as human-readable STL conditions justifying individual predictions, and (ii) global explanations as class-characterising formulae. Experiments demonstrate that STELLE achieves competitive accuracy while providing logically faithful explanations, validated on diverse real-world benchmarks.

JAIR Track: Integration of Logical Constraints in Deep Learning

JAIR Associate Editor: Insert JAIR AE Name

JAIR Reference Format:

Irene Ferfoglia, Simone Silvetti, Gaia Saveri, Laura Nenzi, and Luca Bortolussi*. 2025. Guided by Stars: Interpretable Concept Learning Over Time Series via Temporal Logic Semantics. *Journal of Artificial Intelligence Research* 4, Article 6 (August 2025), 34 pages. doi: [10.1145/nnnnnnnnnnnnnnn](https://doi.org/10.1145/nnnnnnnnnnnnnnn)

1 Introduction

Time series data are pervasive nowadays, arising from systems such as industrial sensor readings, moving through our everyday life via data generated by Internet of Things devices, to safety-critical applications such as digital health equipment and autonomous vehicles. Being able to effectively and efficiently analyse time series is an objective of paramount importance, often tackled by means of data-driven Machine Learning (ML) algorithms (Fawaz et al. 2018; Ruiz et al. 2021). Many of these models are however *black-box*, i.e. the logic behind their outcomes is opaque, hindering their application in high-stakes scenarios, where safety and reliability need to be guaranteed. This lack of transparency raises ethical (Ho 2019; Iman et al. 2021) and legal (European

*Corresponding authors.

Authors' Contact Information: Irene Ferfoglia, ORCID: [0000-0003-1585-6576](https://orcid.org/0000-0003-1585-6576), irene.ferfo@gmail.com, Università degli Studi di Trieste, Trieste, Italy; Simone Silvetti, ORCID: [0000-0001-8048-9317](https://orcid.org/0000-0001-8048-9317), Università degli Studi di Trieste, Trieste, Italy; Gaia Saveri, ORCID: [0009-0003-2948-7705](https://orcid.org/0009-0003-2948-7705), Università degli Studi di Trieste, Trieste, Italy; Laura Nenzi, ORCID: [0000-0003-2263-9342](https://orcid.org/0000-0003-2263-9342), Università degli Studi di Trieste, Trieste, Italy; Luca Bortolussi*, ORCID: [0000-0001-8874-4001](https://orcid.org/0000-0001-8874-4001), lbortolussi@units.it, Università degli Studi di Trieste, Trieste, Italy.



This work is licensed under a Creative Commons Attribution International 4.0 License.

© 2025 Copyright held by the owner/author(s).

DOI: [10.1145/nnnnnnnnnnnnnnn](https://doi.org/10.1145/nnnnnnnnnnnnnnn)

Commission 2016; Helbing 2019) concerns, and undermines human trust despite their state-of-the-art performance across various tasks (Leichtmann et al. 2023). Time series, unlike images, are difficult to interpret by humans, having a hidden semantic that often needs domain knowledge to be grasped. Most existing Explainable Artificial Intelligence (XAI) frameworks for this data type are *post-hoc* (Theissler et al. 2022), i.e. explanations are added on top of a trained model and not computed alongside the predictions of the model itself, and many critical points have been raised about their effectiveness (Turbé et al. 2023).

A suitable formalism for describing time series behaviour and patterns is Signal Temporal Logic (STL) (Maler and Nickovic 2004; Pnueli 1977), which offers a rich yet concise language for expressing properties of signals varying over time. It avoids the vagueness and redundancy of natural language, while still being easy to translate in common words; indeed, STL is the de-facto standard language in Cyber-Physical Systems (CPS) applications (Bartocci, Deshmukh, et al. 2018). One task that received significant attention (Bartocci, Mateis, et al. 2022; Nenzi et al. 2018; Saveri and Bortolussi 2024) is the so-called *requirement mining*, which given a set of (labelled) trajectories aims at extracting a set of STL properties able to discriminate or characterise them. The mined formulae, although exploitable as signal classifiers, only provide a global explanation for the learned decision boundary. Hence STL formulae are valuable candidates to serve as explanations in time series learning algorithms. Following this intuition, we propose a concept-based model (Ghorbani et al. 2019; Yeh et al. 2020) for time series classification, where concepts are represented as STL requirements. Differently from post-hoc XAI methods, our model is *interpretable by design*, as explanations are computed concurrently with the predictions, in the form of succinct sets of STL conditions. Doing so, the outcome of our model is both human-interpretable and able to extract actionable knowledge from the input time series, since the learned concepts can be used to monitor future behaviour of the system or to compare predictions with previous knowledge. Furthermore, an interpretable approach can help meet regulatory requirements, ensuring that the deployment of these technologies adheres to legal standards and ethical guidelines.

Specifically, our contributions consist in: (i) extending the concept of the STL kernel proposed by (Bortolussi et al. 2022) to embed trajectories into STL formulae; (ii) proposing STELLE¹, a concept-based time series classification architecture that directly embeds raw trajectories into a symbolic space of STL formulae through a novel robustness-inspired kernel, enabling end-to-end interpretable classification grounded in temporal logic semantics; (iii) introducing a dual explanation framework that generates both local explanations (as STL formulae justifying individual predictions) and global explanations (as class-characterising temporal patterns) from the same concept space; (iv) demonstrating that STELLE achieves competitive accuracy while maintaining interpretability across diverse real-world benchmarks, including high-dimensional time series data.

The remainder of this paper is organised as follows: Section 2 introduces the necessary background on concept-based learning, explanation by backpropagation, and Signal Temporal Logic and its kernel. Section 3 details proposes our extension of the STL kernel to embed trajectories. Section 4 presents the STELLE framework, detailing its architecture and explanation generation process. In Section 5, the model is evaluated against state-of-the-art methods across both and its interpretability metrics are presented. Lastly, Section 6 discusses related work.

2 Background

+ This section presents the theoretical foundations of our approach. We begin by reviewing concept-based models, which enable interpretable reasoning through human-understandable latent representations, and describe the backpropagation-based technique employed for explanation extraction. We then outline Signal Temporal Logic (STL), a formal language for specifying temporal properties of time series, and discuss its quantitative semantics.

¹Italian term for “stars”

Finally, we describe a kernel formulation for STL that provides a similarity measure between logical specifications, forming the basis for the trajectory embedding kernel used in our architecture.

2.1 Concept-based models

Concept-based models are an emerging paradigm in machine learning that integrate human-understandable concepts into the decision-making process of the model, to make it inherently interpretable (Ghorbani et al. 2019; Yeh et al. 2020). Unlike post-hoc explainability frameworks, which attempt to rationalise black-box predictions after training, concept-based approaches embed semantic representations directly within the learning architecture. These concepts capture meaningful, domain-specific patterns that contribute explicitly to the downstream task.

In the context of time series classification, concepts can correspond to temporal or frequency-based phenomena, such as periodic trends, abrupt changes, local motifs, or statistical features (e.g., amplitude, duration, variability), that experts naturally use to interpret temporal data. By associating model decisions with such interpretable temporal concepts, these frameworks provide insights not only into what the model predicts, but also why certain temporal patterns are deemed discriminative. This paradigm thus bridges the gap between model transparency and performance, enabling more trustworthy and diagnostically useful time series models.

2.2 Explanation by backpropagation

A common family of explanation methods for neural networks is based on the backpropagation of relevance scores from the output layer to the input space. These methods aim to assign an attribution score to each input feature, reflecting its contribution to the model’s prediction. Formally, given a differentiable model $F : \mathbb{R}^d \rightarrow [0, 1]^K$, $\mathbf{x} \mapsto \hat{y}$, K number of classes, the relevance of input dimension x_i for class \hat{y} can be expressed as the partial derivative $\frac{\partial F_{\hat{y}}(\mathbf{x})}{\partial x_i}$, which quantifies local sensitivity. However, simple gradient-based explanations suffer from noise and saturation effects, providing unstable or uninformative attributions.

To mitigate these issues, Sundararajan et al. (2017) introduced *Integrated Gradients* (IG), which compute attributions by integrating the model’s gradients along a continuous path from a baseline input \mathbf{x}' (typically representing “absence of signal”) to the actual input \mathbf{x} . Formally, for the target class \hat{y} , the IG attribution for the i -th feature is defined as:

$$IG_i(\mathbf{x}) = (x_i - x'_i) \int_0^1 \frac{\partial F_{\hat{y}}(\mathbf{x}' + \alpha(\mathbf{x} - \mathbf{x}'))}{\partial x_i} d\alpha$$

This integral captures the cumulative effect of feature x_i on the class score $F_{\hat{y}}$ along the interpolation path between \mathbf{x}' and \mathbf{x} . In this formulation, $\alpha \in [0, 1]$ is a continuous scaling parameter that traces the interpolation path between the baseline input \mathbf{x}' and the actual input \mathbf{x} . When $\alpha = 0$, the model is evaluated at the baseline (typically representing the absence of signal), and when $\alpha = 1$, it is evaluated at the true input. Intermediate values of α correspond to points along the straight line connecting \mathbf{x}' and \mathbf{x} in feature space. The integral thus accumulates the gradient contributions of feature x_i along this path, capturing how changes in x_i influence the model’s output as the input transitions from baseline to actual data.

Integrated Gradients satisfy desirable properties such as *sensitivity* (non-zero attribution for relevant inputs) and *implementation invariance* (consistent results for functionally equivalent networks), making them a robust choice for model interpretability.

In this work, we apply Integrated Gradients not to raw inputs but to the latent concept activations $\mathbf{z}(\mathbf{x})$, yielding class-specific weights $\mathbf{W}_{\hat{y}}$ that quantify the relevance of each concept to the final decision.

2.3 Signal Temporal Logic (STL)

STL is a linear-time temporal logic which expresses properties on trajectories over dense time intervals (Maler and Nickovic 2004). We define as trajectories the functions $\tau : I \rightarrow \mathcal{X}$, where $I \subseteq \mathbb{R}_{\geq 0}$ is the time domain and

$X \subseteq \mathbb{R}^d$, where $d \in \mathbb{N}$ is the state space. The syntax of STL is given by:

$$\varphi := \top \mid \pi \mid \neg\varphi \mid \varphi_1 \wedge \varphi_2 \mid \varphi_1 \mathbf{U}_{[a,b]} \varphi_2$$

where \top is the Boolean *true* constant; π is an *atomic predicate*, interpreted as a function of the form $f_\pi(\mathbf{x}) \geq 0$ over variables $\mathbf{x} \in \mathbb{R}^N$ (we refer to N as the number of variables of a STL formula, i.e. individual signals used as arguments of the atomic predicates); negation \neg and conjunction \wedge are the standard Boolean connectives, and \mathbf{U}_I is the *Until* temporal modality, where $[a, b] \subseteq I$ is a real positive interval. We can derive the disjunction operator \vee from \wedge and \neg via De Morgan's law as $\varphi_1 \vee \varphi_2 = \neg(\neg\varphi_1 \wedge \neg\varphi_2)$, the *Eventually* $\mathbf{F}_{[a,b]}$ and *Always* $\mathbf{G}_{[a,b]}$ operators from the Until temporal modality as $\mathbf{F}_{[a,b]} \varphi = \top \mathbf{U}_{[a,b]} \varphi$ and $\mathbf{G}_{[a,b]} \varphi = \neg \mathbf{F}_{[a,b]} \neg\varphi$, respectively.

We can intuitively interpret the temporal operators over a time interval $[a, b]$ as:

- *Eventually*: a property is eventually satisfied if it is satisfied at some point inside $[a, b]$;
- *Globally*: a property is globally satisfied if it is true continuously in the future in the specified temporal interval;
- *Until*: it captures the relationship between two conditions φ, ψ in which the first condition φ holds until, at some point in $[a, b]$ in the future, ψ becomes true.

We call \mathcal{P} the set of well-formed STL formulae; we refer to the number of symbols of an STL formula as its number of nodes, and to the maximum number of allowed signals dimension over which it can be interpreted as the number of its variables. For example, the sentence “the temperature τ of the room will reach 25 degrees within the next 10 minutes and will stay above 22 degrees for the following 60 minutes” translates in STL as $\mathbf{F}_{[0,10]}(\tau \geq 25 \wedge \mathbf{G}_{[0,60]} \tau \geq 22)$.

2.3.1 Robustness. STL has both a qualitative (or Boolean) and a quantitative (or robust) semantics (Donzé et al. 2013). While the Boolean semantics gives the classical notion of satisfaction, the robustness of a formula φ on a signal τ is a value $\rho(\varphi, \tau, t) \in \mathbb{R} \cup \{-\infty, +\infty\}$ quantifying the *robustness degree* of the property φ on the trajectory τ at time t . Intuitively, robustness generalises Boolean satisfaction by measuring not only whether a formula holds, but also how strongly it is satisfied or violated. Positive robustness values indicate that φ is satisfied with a safety margin, whereas negative values quantify the extent of its violation. Its sign provides the link with the standard Boolean semantics, in that a signal τ satisfies an STL formula φ at a time t iff the robustness degree $\rho(\varphi, \tau, t) \geq 0$. Its absolute value, instead, can be interpreted as a measure of the distance to violation or satisfaction of φ on τ . Robustness is recursively defined as:

$$\begin{aligned} \rho(\pi, \tau, t) &= f_\pi(\tau(t)) \quad \text{for } \pi(\mathbf{x}) = (f_\pi(\mathbf{x}) \geq 0) \\ \rho(\neg\varphi, \tau, t) &= -\rho(\varphi, \tau, t) \\ \rho(\varphi_1 \wedge \varphi_2, \tau, t) &= \min(\rho(\varphi_1, \tau, t), \rho(\varphi_2, \tau, t)) \\ \rho(\varphi_1 \mathbf{U}_{[a,b]} \varphi_2, \tau, t) &= \max_{t' \in [t+a, t+b]} \left(\min_{t'' \in [t, t']} \rho(\varphi_1, \tau, t'') \right) \end{aligned}$$

For completeness, we report also the definition of robustness of derived temporal operators:

$$\begin{aligned} \text{eventually } \rho(\mathbf{F}_{[a,b]} \varphi, \tau, t) &= \max_{t' \in [t+a, t+b]} \rho(\varphi, \tau, t') \\ \text{always } \rho(\mathbf{G}_{[a,b]} \varphi, \tau, t) &= \min_{t' \in [t+a, t+b]} \rho(\varphi, \tau, t') \end{aligned}$$

Throughout the paper, we will consider this metric at $t = 0$ and simplify the notation to $\rho(\varphi, \tau)$. A distribution Γ over STL formulae can be constructed procedurally by recursively expanding syntax trees, where each node has

a fixed probability of being instantiated as an atomic predicate, and the remaining cases are uniformly sampled from the available temporal and logical operators (Saveri, Nenzi, et al. 2024).

2.4 A kernel for STL

A kernel for STL that leverages the quantitative semantics of STL (Bortolussi et al. 2022) can be used for finding continuous representations of STL formulae. Indeed, robustness in this context allows formulae to be treated as functionals that map trajectories into real numbers i.e. $\rho(\varphi, \cdot) : \mathcal{T} \rightarrow \mathbb{R}$ such that $\tau \mapsto \rho(\varphi, \tau)$. By considering these functionals as feature maps and fixing a probability measure μ_0 on the trajectory space \mathcal{T} , a kernel function that captures the similarity between STL formulae φ and ψ can be defined as follows:

$$k(\varphi, \psi) = \langle \rho(\varphi, \cdot), \rho(\psi, \cdot) \rangle = \int_{\tau \in \mathcal{T}} \rho(\varphi, \tau) \rho(\psi, \tau) d\mu_0(\tau) \quad (1)$$

This approach enables the use of the scalar product in the Hilbert space L^2 as a kernel for \mathcal{P} . Essentially, this kernel yields a high positive value for formulae that behave similarly on high-probability trajectories w.r.t. μ_0 , and a low negative value for formulae that disagree on those trajectories. Further details about the STL kernel are provided in Appendix A.

This kernel establishes the mathematical foundation for our framework by enabling two key capabilities: (i) quantifying semantic similarity between temporal logic formulae through their behavioural profiles, and (ii) providing the theoretical bridge between symbolic reasoning and continuous embedding spaces that we exploit for trajectory-formula alignment. While the original formulation measures formula-formula similarity, we extend this core definition to develop our trajectory embedding mechanism, maintaining interpretability through shared semantic grounding in STL robustness.

3 Trajectory embedding kernel

The first contribution of this work is the definition of a trajectory embedding kernel that enables the representation of raw time series data within the same interpretable space as logical formulae. This kernel constitutes a fundamental component of the proposed architecture, as it allows the model to jointly reason over trajectories and temporal logic concepts.

While the STL kernel described in Section 2.4 enables the embedding of logical formulae, it is key to our goal to embed raw input trajectories into the same interpretable space. To achieve this, we define a trajectory-specific kernel inspired by STL robustness. A kernel for input trajectories can be defined in the same functional space as STL formulae by extending the concept of robustness to measure similarity between trajectories. Given a reference trajectory $\tau \in \mathcal{T}$, we define a function $\rho_\tau : \mathcal{T} \rightarrow \mathbb{R}$ that quantifies the similarity between τ and another trajectory $\xi \in \mathcal{T}$. A natural choice for this function is

$$\rho_\tau(\xi) = d_\tau(\xi)/\varepsilon \quad \text{where} \quad d_\tau(\xi) = \|\xi - \tau\|_2^2 \quad (2)$$

is the squared L_2 distance and $\varepsilon > 0$ controls the locality of the similarity measure. By interpreting ρ_τ as a trajectory-dependent functional analogous to the robustness of an STL formula, we can define a kernel between a trajectory τ and an STL formula φ as:

$$k(\tau, \varphi) = \int_{\xi \in \mathcal{T}} \rho_\tau(\xi) \rho(\varphi, \xi) d\mu_0(\xi) \quad (3)$$

This formulation has three critical properties: (i) trajectories and formulae occupy a shared semantic space where distances reflect behavioural alignment, (ii) the kernel inherits the STL kernel's theoretical guarantees, and (iii) all subsequent operations remain grounded in temporal logic semantics. Section 4.2 depicts how STELLE

exploits this through direct concept-based embedding, avoiding intermediate representations while preserving interpretability.

4 The model

We now introduce STELLE (Signal Temporal logic Embedding for Logically-grounded Learning and Explanation), a novel architecture for interpretable time series classification. STELLE operates by projecting input trajectories into a semantic space defined by a diverse set of human-interpretable Signal Temporal Logic (STL) concepts. The model learns to classify by attending to these concepts and assessing how unusually they are satisfied relative to different classes. This design inherently provides explanations: local predictions are justified by a concise logical combination of relevant temporal patterns, while global class characterisations are derived by aggregating these local explanations into discriminative formulae. The following subsections detail the construction of the concept set, the STELLE architecture, and the procedures for extracting both local and global explanations.

4.1 Concept set

In our model, concepts are defined as temporal logic conditions expressed using STL formulae, which encapsulate human-interpretable patterns over time. These logical expressions serve both as interpretable units of explanation and as semantic anchors in the shared embedding space.

To build a semantically rich yet interpretable concept set, we generate STL formulae by sampling from a space of symbolic templates. Each formula is instantiated from a probabilistic grammar with a bounded number of variables and a maximum number of nodes, ensuring syntactic simplicity and human interpretability. These candidate formulae are evaluated over a fixed dataset of time series signals using quantitative semantics, resulting in robustness signature vectors that capture their behaviour across trajectories.

Concept selection proceeds incrementally: at each step a batch of new candidates is sampled and evaluated, and those whose signatures differ significantly from the existing set are retained, measured via cosine similarity. To promote parsimony, structurally simpler formulae are preferred when behavioural redundancy is detected among candidates. This process continues until the desired number of concepts is reached. Importantly, a concept set is generated once using a fixed temporal window, and the resulting STL formulae can later be linearly rescaled to accommodate datasets of varying lengths by adjusting their temporal thresholds proportionally.

This process guarantees that the selected formulae are both representative and diverse, and that they span a broad range of temporal patterns observed in the data. We refer the reader to Appendix B for a more detailed explanation of the procedure.

4.2 Architecture

Our architecture, STELLE, is designed to perform interpretable time series classification through concept-based reasoning. It integrates symbolic information from Signal Temporal Logic (STL) with trajectory representations, enabling explanations that are grounded in logical temporal behaviours. The architecture, depicted in Figure 1, consists of three components: (i) a trajectory embedding, (ii) a discriminability mechanism, and (iii) a learned concept relevance module.

The model supports an arbitrary number of classes, enabling it to scale naturally to multiclass classification tasks, and each formula may involve one or more signal dimensions, allowing the model to express and attend to complex relationships in multivariate inputs.

Trajectory embedding. A key innovation of our architecture lies in the use of a robustness-inspired kernel for input trajectories introduced in Section 3, which enables their projection into the same logic-grounded space as STL formulae.

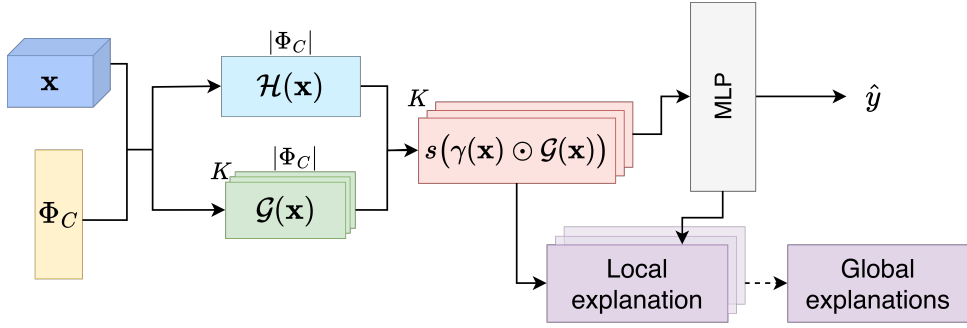


Fig. 1. STELLE architecture. Input trajectories \mathbf{x} are embedded via STL concepts formulae Φ_C , creating $\mathcal{H}(\mathbf{x})$. This gets scaled, creating $\gamma(\mathbf{x})$, and integrated with class-specific scores $\mathcal{G}(\mathbf{x})$ for classification \hat{y} and generation of local explanations, which can be aggregated into global explanations.

We begin by defining a fixed set of STL formulae $\Phi_C = \{\varphi_1, \dots, \varphi_C\}$ that represent high-level, human-interpretable concepts, as described in Section 4.1. Given an input time series \mathbf{x} , we compute its embedding $\mathcal{H}(\mathbf{x}) \in \mathbb{R}^C$ by evaluating the robustness of \mathbf{x} with respect to each concept formula $\varphi_i \in \Phi_C$, as described in Section 3. This results in a concept-based representation of the trajectory, where each dimension quantifies the degree to which the corresponding temporal property is satisfied. The resulting embedding is fully interpretable, as each component is tied to a known STL formula.

Discriminability scores. To assess the explanatory value of each concept, we compute class-specific discriminability scores based on robustness statistics. Let K be the number of classes, and let k denote a specific class. For each concept $\varphi_i \in \Phi_C$, we measure how atypical its satisfaction is for the input trajectory when compared to other classes. We define the discriminability matrix $\mathcal{G}(\mathbf{x}) \in [0, \infty)^{C \times K}$, where each entry $\mathcal{G}_i^k(\mathbf{x})$ is computed as

$$\mathcal{G}_i^k(\mathbf{x}) = \frac{|\rho(\varphi_i, \mathbf{x}) - \mu_{k^*,i}|}{\sigma_{k^*,i} + \varepsilon_G}$$

Here, $\rho(\varphi_i, \mathbf{x})$ denotes the robustness of the input trajectory \mathbf{x} with respect to formula φ_i , ε_G is a small regularisation constant, and $\mu_{k^*,i}$, $\sigma_{k^*,i}$ are the mean and standard deviation of robustness values for class $k^* \neq k$. This normalisation highlights the extent to which each formula supports or contradicts the model's prediction relative to the distribution of robustness in the competing classes.

Learned concept relevance. To identify the most relevant concepts for each input, we compute concept selection scores that determine their relative importance. Specifically, we generate raw selection weights as:

$$\gamma(\mathbf{x}) = \mathcal{H}(\mathbf{x})/T \in \mathbb{R}^C \quad (4)$$

where T is a temperature parameter controlling the sharpness of the selection. We standardise the trajectory embeddings $\mathcal{H}(\mathbf{x})$ before computing $\gamma(\mathbf{x})$ to ensure stable and comparable concept weighting across samples. This normalisation step prevents scale disparities among embeddings from dominating the relevance computation. In contrast, $\mathcal{G}(\mathbf{x})$ is left unstandardised, as its values are already expressed in a relative scale that captures concept distinctiveness across classes, and rescaling it would distort its interpretive meaning.

These selection weights are then used to modulate the class-specific discriminability scores through an element-wise normalisation operation, producing the combined representation:

$$\begin{aligned} \mathbf{z}(\mathbf{x}) &= \gamma(\mathbf{x}) \odot \mathcal{G}(\mathbf{x}) & \in [0, \infty)^{C \times K} \\ \bar{\mathbf{z}}(\mathbf{x}) &= s(\mathbf{z}(\mathbf{x})) & \in (-1, 1)^{C \times K} \end{aligned} \quad (5)$$

where \odot is the Hadamard product s is the Softsign activation function. This formulation ensures that the modulated concepts reflect both their relative relevance to the input and their class-specific explanatory strength.

The resulting matrix $\bar{\mathbf{z}}(\mathbf{x})$ is flattened and passed through an MLP to produce the final classification logits.

This architecture achieves interpretability in two complementary ways. First, the learned relevance weights $\gamma(\mathbf{x})$ identify which STL concepts contribute most strongly to the decision. Second, the discriminability scores $\mathcal{G}(\mathbf{x})$ explain why those concepts support or contradict the model's prediction, by quantifying how unusual their satisfaction is for the predicted class compared to others. Combined, these two components provide both concept-level attribution and class-level reasoning, enabling explanations that are both local (specific to individual trajectories) and global (aggregated across the dataset). This dual interpretability allows STELLE to not only highlight the temporal patterns driving a particular prediction but also to characterise the broader logic underlying each class.

4.3 Explanation extraction

The explanation generation synthesises information from three components: (i) the selection weights $\gamma(\mathbf{x})$ identifying relevant concepts, (ii) the discriminability scores $\mathcal{G}(\mathbf{x})$ measuring concept atypicality, and (iii) the backpropagated classifier weights \mathbf{W} determining each concept's importance to the final prediction.

4.3.1 Local explanations. For a given input trajectory \mathbf{x} and a target class k , local explanations quantify the contribution of each concept φ_i to the model's confidence in class k . We first compute the class-specific latent representation of $\mathbf{z}(\mathbf{x})$ as defined in Equation 5, where $\mathbf{z}(\mathbf{x})_k \in [0, \infty)^C$ denotes the vector of concept activations for \mathbf{x} wrt class k , and C is the total number of STL concepts. The index $k \in 1, \dots, K$ selects the subspace corresponding to the target class.

To estimate how each concept influences the class score, we employ *Integrated Gradients* (see Section 2.2) to backpropagate relevance from the classifier output to the latent concept dimensions. Let $F : \mathbb{R}^C \rightarrow [0, 1]^K$ denote the classification head mapping latent concept activations to class probabilities. For class k , the relevance of each latent input dimension z_i is computed as:

$$W_{k,i} = (z_i - z'_i) \int_0^1 \frac{\partial F_k(\mathbf{z}' + \alpha(\mathbf{z} - \mathbf{z}'))}{\partial z_i} d\alpha$$

where \mathbf{z}' is a baseline latent input (set to the zero vector), and F_k is the classifier output corresponding to class k . The resulting relevance weights \mathbf{W}_k are normalised to $[0, 1]$, providing a smooth and faithful attribution of each concept's influence on F_k .

Importantly, the attributions are backpropagated to the *non-normalised* matrix $\mathbf{z}(\mathbf{x})$, rather than its soft-signed version $\bar{\mathbf{z}}(\mathbf{x})$. This ensures that gradient propagation is not distorted by the bounded Softsign activation, which would otherwise attenuate large-magnitude responses and compress their relative importance. By operating directly on $\mathbf{z}(\mathbf{x})$, we preserve the true scale of the underlying concept activations, yielding explanations that more accurately reflect their quantitative influence on the prediction.

The final explanation vector is computed using a discriminative scoring mechanism that identifies concepts most distinctive to each class. For an input trajectory \mathbf{x} and target class k , the concept-class activation matrix

$\mathbf{A}(\mathbf{x}) \in \mathbb{R}^{C \times K}$, where C is the cardinality of the concept set and K is the number of classes, is defined as

$$\mathbf{r}(\mathbf{x})_k = \left| \mathbf{A}_{:,k}(\mathbf{x}) - \frac{1}{K-1} \sum_{k' \neq k} \mathbf{A}_{:,k'}(\mathbf{x}) \right|$$

where $\mathbf{A}_{:,k}(\mathbf{x})$ denotes the vector of concept activations for the predicted class k , and the summation term represents the mean activation vector across all other classes. This formulation identifies concepts that exhibit substantially different activation patterns between the target class and alternative classes, thereby highlighting the most discriminative concepts for each classification decision and yielding interpretable, concept-level local explanations.

To identify the most influential concepts, two selection strategies are supported. If a fixed budget $\bar{y} \in \mathbb{N}$ is specified, the top- \bar{y} concepts with highest absolute relevance scores $|\mathbf{r}|$ are selected. Otherwise, we apply a cumulative relevance cut-off: the entries of $|\mathbf{r}|$ are sorted, and the smallest prefix whose cumulative sum reaches a target fraction $\bar{y}_t \in (0, 1]$ of the total relevance is retained. This allows the explanation size to adapt to the complexity of the input.

Let $\mathcal{F}_x = \{\varphi_1, \dots, \varphi_{|\mathcal{F}_x|}\}$ be the selected concepts. Each φ_i is subsequently refined to enhance interpretability by adjusting its thresholds, polarity, and syntactic complexity, as will be detailed in Section 4.3.3. Moreover, a threshold $\bar{y}_\ell \in [0, 1)$ controls the trade-off between formula complexity (node count) and classification fidelity: lower values prioritise classification accuracy over interpretability, allowing longer formulae that marginally improve performance. The result is a set of simplified formulae \mathcal{F}'_x . We define the local explanation for input \mathbf{x} with reference to target class \hat{y} as:

$$E_\ell(\mathbf{x}, \hat{y}) = \bigwedge_{\varphi'_i \in \mathcal{F}'_x} \varphi'_i$$

This logical expression provides a sufficient condition for describing class \hat{y} . Each conjunct represents a distinct, human-readable behavioural property. Together, they provide a faithful and compact explanation of the model's decision. Finally, the resulting formula goes through a logic-aware and data-aware pruning to remove uninformative predicates and improve its readability. We refer the reader to Appendix C for more details about the process.

4.3.2 Global explanations. Global explanations aim to characterise, for each class k , the symbolic conditions that best describe its underlying temporal behaviour. Rather than aggregating only the explanations from correctly predicted test samples, we construct class-level formulae using the training trajectories and their true labels. This choice ensures that global explanations reflect intrinsic class semantics rather than potential model-specific biases introduced during prediction. In addition, since robustness evaluations are precomputed for all training trajectories, the explanation set can be efficiently updated when new data become available without retraining the full model.

For each class k , we collect all local explanations associated with the corresponding training trajectories:

$$\mathcal{F}_k = \{E_\ell(\mathbf{x}, k) \mid \mathbf{x} \in \mathcal{T}_{\text{train}}, y(\mathbf{x}) = k\},$$

where $E_\ell(\mathbf{x}, k)$ denotes the local explanation extracted for class k given input \mathbf{x} , $\mathcal{T}_{\text{train}}$ is the training set and $y : \mathcal{T}_{\text{train}} \rightarrow \mathbb{N}$, $y(\mathbf{x})$ is the true class of \mathbf{x} . Each local explanation $E_\ell(\mathbf{x}, k)$ consists of one STL formula φ_i whose robustness values are most discriminative for that sample.

To identify which of these formulae exhibit general class-level relevance, we construct a division matrix $D^k \in \{0, 1\}^{|\mathcal{F}_k| \times |\mathcal{F}_k|}$, where:

$$D_{ij}^k = \begin{cases} 1, & \text{if } \rho(\varphi_j, \mathbf{x}_i) \notin [\min_{\mathbf{x} \notin y^{-1}(k)} \rho(\varphi_j, \mathbf{x}), \max_{\mathbf{x} \notin y^{-1}(k)} \rho(\varphi_j, \mathbf{x})] \\ 0, & \text{otherwise} \end{cases}$$

and $y^{-1}(k) = \{\mathbf{x} \in \mathcal{T}_{train} \mid y(\mathbf{x}) = k\}$.

This criterion ensures that a formula φ_i is considered discriminative for class k if its robustness values on class- k trajectories lie outside the range observed in all non-class- k samples. The division matrix therefore quantifies, across all training data, which formulae distinctly separate the target class from the others.

Next, we seek a minimal subset of formulae $\mathcal{F}'_k \subseteq \mathcal{F}_k$ that jointly covers (i.e., distinguishes) all or most class- k samples. To formalise this, we define a minimum-cost set cover problem:

$$\min_{\mathbf{c}} \sum_i c_i \cdot \text{cost}(\varphi_i) \quad \text{s.t.} \quad D^k \mathbf{c} \geq \bar{y}_g \mathbf{1}, \quad c_i \in \{0, 1\},$$

where \mathbf{c} is a binary selection vector indicating which formulae are included in the final global explanation, $\text{cost}(\varphi_i)$ corresponds to the syntactic complexity (e.g., node count) of φ_i , and $\bar{y}_g \in [0, 1]$ relaxes the coverage constraint to allow simpler, approximate global explanations. This optimisation is cast as a 0–1 Integer Linear Program (ILP). When the ILP becomes infeasible or too computationally expensive, we revert to a combinatorial search that greedily selects formulae whose disjunction maximises class separability while minimising redundancy.

The resulting symbolic explanation for class k is expressed as:

$$E_g(k) = \bigvee_{\varphi_i \in \mathcal{F}'_k} \varphi_i,$$

representing a sufficient logical condition for class membership, i.e. any trajectory satisfying at least one φ_i in \mathcal{F}'_k is typically assigned to class k .

Crucially, this construction allows the global explanations to be incrementally refined: as new trajectories become available, robustness statistics and coverage relations can be updated without retraining, ensuring that $E_g(k)$ remains representative of the evolving data distribution. As in the local case, the final selected formulae undergo logic-aware and data-aware simplification to maximise readability while preserving discriminative and semantic consistency.

4.3.3 Improving readability. To improve the readability and discriminative utility of learned STL formulae, we apply three complementary post-processing strategies. First, logical simplification rewrites formulae by eliminating redundant or structurally equivalent expressions based on syntactic rules (e.g., removing double negations, flattening nested temporal operators). Second, we apply threshold adjustment and ensure consistent satisfaction by negating the formula if it does not hold for the trajectories to explain, exploiting the linearity of robustness with respect to atomic thresholds to refine the decision boundary. By tuning thresholds and optionally negating formulae, we ensure that the resulting expression better separates the target and maintains interpretability. Lastly, data-aware simplification uses empirical evaluations over the trajectories to simplify subformulae that are uniformly true or false, enabling semantic reduction beyond structural rules.

For example, the formula

$$\neg(\mathbf{G}_{[0,20]}(\mathbf{G}_{[5,10]}(x_0 \leq 0.3)))$$

is progressively refined to

$$\begin{aligned} &\neg(\mathbf{G}_{[5,30]}(x_0 \leq 0.3)) \\ &\mathbf{F}_{[5,30]}(x_0 > 0.3) \end{aligned}$$

through logical simplification.

Each method is independently applicable and contributes to enhancing clarity, compactness, and class-specific relevance. Full details rules and algorithms are presented in Appendix C.

Table 1. Summary of the multivariate time series datasets used in the experimental evaluation. Each dataset is identified by a short two-letter code (ID). The dataset type denotes the domain of the recorded signals.

Dataset	ID	TrainSize	TestSize	Length	#Classes	Type	Channels
ArticularyWordRecognition	AW	275	300	144	25	MOTION	9
AtrialFibrillation	AF	15	15	640	3	ECG	2
BasicMotions	BM	40	40	100	4	HAR	6
Cricket	CR	108	72	1197	12	HAR	6
ERing	ER	30	270	65	6	HAR	4
Epilepsy	EP	137	138	207	4	HAR	3
EthanolConcentration	EC	261	263	1751	4	SPECTRO	3
HandMovementDirection	HD	160	74	400	4	EEG	10
Handwriting	HW	150	850	152	26	HAR	3
Libras	LI	180	180	45	15	HAR	2

5 Experimental evaluation

We evaluate STELLE on a subset of multivariate time series classification tasks from the University of East Anglia (UEA) Time Series Archive (Bagnall, Dau, et al. 2018), a comprehensive benchmark suite spanning a wide range of domains, including physiological measurements, motion capture sequences, environmental sensor readings, and spectrographic signals. To construct a representative yet computationally tractable benchmark, we selected the first ten datasets in alphabetical order from the archive, excluding *DuckDuckGeese*, which was omitted due to its extremely high dimensionality (over 1000 variables) exceeding the available computational resources. Table 1 summarises the key characteristics of the selected datasets, including their short identifiers, size, sequence length, number of classes, and signal dimensionality. The *Type* column indicates the application domain of each dataset: MOTION (motion capture), ECG (electrocardiography), HAR (Human Activity Recognition), SPECTRO (spectrographic signals) and EEG (electroencephalography).

After a first hyperparameter tuning performed on a few representative datasets, a number of hyperparameters were fixed, including batch size, the initialisation of ε_G , and the learning rates for both the latter and the temperature parameter T . Moreover, we fixed $\bar{\gamma}_t$ for explanation extraction and all the parameters regarding concept creation. For the remaining ones, due to the highly diverse nature of the datasets, we chose to fine-tune them tailored to each problem.

For more information about training details, we refer the reader to Appendix D. All code and scripts for reproducing our experiments are available at <https://github.com/ireneferfo/STELLE>.

Baselines. To contextualise STELLE’s performance, we compare it against a broad selection of state-of-the-art TSC methods. These include deep learning architectures such as InceptionTime (Ismail Fawaz et al. 2020), ResNet (Fawaz et al. 2018), TapNet (Zhang et al. 2020), and the HIVE-COTE 2.0 components HC1 (Bagnall, Flynn, et al. 2020) and HC2 (Middlehurst, Large, Flynn, et al. 2021). We also consider transform-based methods including ROCKET (Dempster et al. 2020), Arsenal and DrCIF (Middlehurst, Large, Flynn, et al. 2021), as well as distance-based approaches using dynamic time warping (1NN-DTW-D, 1NN-DTW-I, 1NN-DTW-A (Mizuhara et al. 2006)). The comparison also includes symbolic and feature-based methods such as TSF (Deng et al. 2013), CIF (Middlehurst, Large, and Bagnall 2020), TDE (Middlehurst, Large, Cawley, et al. 2021), STC (Hills et al. 2014), MrSEQL (Nguyen et al. 2019), MUSE (Schäfer and Leser 2018), cBOSS (Middlehurst, Vickers, et al. 2019), and RSF (Karlsson et al. 2016), which offer partial interpretability through engineered symbolic or interval features,

though without explicit semantic explanations. We use performance metrics reported in Ruiz et al. (2021), which represents the most comprehensive recent benchmark on the UEA multivariate archive.

Evaluation metrics. To comprehensively evaluate both predictive performance and interpretability, we employ a set of quantitative metrics spanning classification, explanation efficiency and readability, and computational efficiency.

For explanation evaluation, we analyse both *local* and *global separability*. For each local explanation $E_\ell(\mathbf{x}, k)$, separability quantifies how well the explanation distinguishes between the target trajectory's class and all other classes. Specifically, for a target trajectory \mathbf{x} we compute:

$$\text{Sep}(E_\ell(\mathbf{x}, k)) = \frac{\#\{y(\tau) \notin k : \text{sign}(\rho(E_\ell(\mathbf{x}, k), \tau)) \neq \text{sign}(\rho(E_\ell(\mathbf{x}, k), \mathbf{x}))\}}{\#\{y(\tau) \notin k\}} \times 100, \quad (6)$$

where $E_\ell(\mathbf{x}, k)$ denotes the local explanation extracted for class k , τ represents trajectories from the training dataset \mathcal{T}_{train} , and $y : \mathcal{T} \rightarrow \mathbb{N}$ maps trajectories to the target label. This represents the percentage of trajectories from the opposite class whose robustness sign differs from that of the target trajectory, where τ denotes a trajectory from the set of all trajectories not belonging to class k . A high separability value indicates that the explanation generalises well to unseen samples of the same class and excludes those from other classes.

We report the mean standard deviation of local separability under different filtering conditions: (i) only for correctly classified samples (reflecting explanation reliability), (ii) only for misclassified samples, analysed from two distinct perspectives: explanations generated with respect to the true class and with respect to the predicted class. Explanations generated with respect to the true class reveal whether the model's reasoning aligns with actual class characteristics, measuring how well the explanation captures the true class's distinguishing features. Low separability here indicates a misalignment between the model's reasoning and ground truth. On the other hand, explanations generated with respect to the predicted class expose the flawed logic used to justify incorrect decisions, revealing what misleading patterns or correlations the model relies on when making errors. Analysing both perspectives provides comprehensive insight into explanation failure modes and model robustness.

For global explanations, we compute class separability both per-class and overall. The *per-class separability* for class k is given by:

$$\text{Sep}_k(E_g(k)) = \frac{TP_k + TN_k}{\text{total}_k},$$

where TP_k and TN_k respectively denote trajectories of class k that satisfy the class explanation $E_g(k)$ and trajectories of other classes that do not satisfy it.

The *overall separability* is obtained by micro-averaging across all classes:

$$\text{Sep} = \frac{\sum_k (TP_k + TN_k)}{\sum_k \text{total}_k}, \quad (7)$$

representing the total proportion of trajectories correctly classified by their respective class explanations.

We evaluate both measures under three conditions: the entire test set, only correctly classified samples, and only misclassified samples. This allows us to analyse how consistently the explanations reflect the model's decisions.

Finally, to assess interpretability and efficiency, we measure *readability* (in terms of the number of syntactic nodes and distinct variables per formula), training time, inference time, and explanation extraction time. Together, these metrics provide a balanced assessment of both model performance and the interpretability-efficiency trade-off.

Table 2. Comparative performance analysis of STELLE against state-of-the-art time series classification methods on the UEA multivariate archive. The table presents classification accuracy scores with best results emphasised for easy comparison. The column “Mean” indicates the average performance of all baseline classifiers for each dataset, providing a reference for comparative ranking. Abbreviations used are: DTW-D (*1NN-DTW-D*), DTW-I (*1NN-DTW-I*), and DTW-A (*1NN-DTW-A*). Performance metrics sourced from Ruiz et al. (2021).

Dataset	DTW-D	ROCKET	STC	TapNet	HC2	DrCIF	DTW-I	Arsenal	RISE	MrSEQL	STELLE
AW	0.99	1.0	0.98	0.97	1.0	0.98	0.94	1.0	0.96	0.99	0.95
AF	0.24	0.25	0.32	0.3	0.28	0.23	0.35	0.26	0.24	0.37	0.33
BM	0.95	0.99	0.98	0.99	0.99	1.0	0.72	0.99	1.0	0.95	0.96
CR	1.0	1.0	0.99	0.97	1.0	0.99	0.96	1.0	0.98	0.99	0.88
ER	0.93	0.98	0.84	0.89	0.99	0.98	0.91	0.98	0.82	0.93	0.84
EP	0.96	0.99	0.99	0.96	1.0	0.99	0.67	0.99	1.0	1.0	0.94
EC	0.3	0.45	0.82	0.29	0.79	0.67	0.31	0.48	0.49	0.6	0.32
HD	0.3	0.45	0.35	0.32	0.4	0.46	0.27	0.45	0.28	0.35	0.27
HW	0.61	0.57	0.29	0.33	0.56	0.34	0.34	0.55	0.18	0.54	0.2
LI	0.88	0.91	0.84	0.84	0.93	0.91	0.79	0.89	0.82	0.87	0.71
Mean	0.72	0.76	0.74	0.69	0.79	0.76	0.63	0.76	0.68	0.76	0.64
Dataset	MUSE	InceptionT	HC1	cBOSS	ResNet	TSF	TDE	DTW-A	CIF	RSF	Mean
AW	0.99	0.99	0.98	0.98	0.98	0.95	0.98	0.99	0.98	0.98	0.95
AF	0.74	0.22	0.29	0.3	0.36	0.3	0.3	0.22	0.25	0.28	0.31
BM	1.0	1.0	1.0	0.99	1.0	1.0	0.99	1.0	1.0	1.0	0.98
CR	1.0	0.99	0.99	0.98	0.99	0.93	0.99	1.0	0.98	0.97	0.98
ER	0.97	0.92	0.94	0.84	0.87	0.9	0.94	0.93	0.96	0.92	0.84
EP	1.0	0.99	1.0	1.0	0.99	0.97	1.0	0.97	0.98	0.96	0.97
EC	0.49	0.28	0.81	0.4	0.29	0.45	0.53	0.3	0.73	0.34	0.49
HD	0.38	0.42	0.38	0.29	0.35	0.49	0.38	0.31	0.52	0.32	0.37
HW	0.52	0.66	0.5	0.49	0.6	0.36	0.56	0.61	0.35	0.37	0.47
LI	0.9	0.89	0.9	0.85	0.94	0.8	0.88	0.88	0.92	0.76	0.87
Mean	0.8	0.74	0.78	0.71	0.74	0.72	0.76	0.72	0.77	0.69	0.73
											0.64

5.1 Results

We evaluate STELLE on ten benchmark datasets from the UEA Time Series Archive (Bagnall, Dau, et al. 2018), comparing it against both state-of-the-art and classical baselines introduced in earlier. The evaluation follows a protocol of 10 folds with 3 seeds each (30 total runs per dataset), consistent with the experimental setup used to obtain the baseline performances reported in Ruiz et al. (2021). All experiments were executed on a DELL PowerEdge R7525 server equipped with dual AMD EPYC 7542 CPUs (32 cores each), 768 GB RAM, and two NVIDIA A100 GPUs. The GPU resources were partitioned, with each run typically using up to 10 GB of GPU memory, and at most 20 GB for the largest datasets. CPU memory usage ranged between 20 GB and 150 GB, with only two datasets requiring allocations above 50 GB. Across datasets, STELLE achieves moderate yet consistent performance. While it does not rank among the top-performing methods in terms of raw accuracy, it maintains stable results across diverse domains, including motion capture, physiological signals, and spectrographic data. For instance, on datasets such as *ArticularyWordRecognition* (AW) and *Epilepsy* (EP), its performance approaches that of ensemble-based methods such as HC2 and DrCIF, whereas on more complex, high-dimensional tasks,

such as *HandMovementDirection* (HD) and *EthanolConcentration* (EC) its accuracy remains competitive despite the additional interpretability constraints.

It is worth emphasising that STELLE is the only inherently interpretable method among all compared approaches. Whereas existing neural and ensemble models (e.g., ROCKET, InceptionTime, ResNet, HC2) provide no direct insight into their decision processes and require external post-hoc explainers, STELLE produces symbolic explanations natively, in the same formal language, Signal Temporal Logic, used for reasoning. Moreover, to the best of our knowledge, it is the first model to provide both local (trajectory-specific) and global (class-level) logical explanations for multivariate time series.

Although a trade-off between interpretability and accuracy is expected, STELLE demonstrates that meaningful, formally grounded explanations can be obtained without a substantial loss in predictive performance if compared with black-box SOTA algorithms. Its stability across datasets suggests that the proposed robustness-based representation captures general temporal properties that extend beyond dataset-specific patterns.

Table 2 provides a comprehensive comparison of classification accuracy across all benchmark datasets, with STELLE’s performance highlighted for direct comparison against these state-of-the-art methods. The table shows mean accuracy rankings that demonstrate STELLE’s positioning within the current TSC landscape.

5.2 Explanatory performance

In addition to evaluating predictive accuracy, we assessed the interpretability of the explanations generated by STELLE for three representative datasets, *BasicMotions* (BM), *ERing* (ER), and *Epilepsy* (EP), chosen as examples where STELLE’s analysis completed most efficiently. We fixed the parameters introduced in Section 4.3 $\bar{\gamma}_t = 0.8$ to retain only the most relevant concepts and $\bar{\gamma}_e = \bar{\gamma}_g = 0$ in order to prioritise classification accuracy over interpretability. This configuration maximises local separability (Equation 6), allowing us to analyse the structural properties of the formulae without interpretability constraints. In particular, all learned formulae achieve perfect local separability scores in all evaluated cases.

Tables 3 and 4 report, respectively, the mean number of syntactic nodes and distinct variables in the local explanations before and after postprocessing, computed across all runs used to extract the classification accuracy reported earlier, distinguishing between correctly classified trajectories (*C*), misclassified trajectories with explanations extracted with respect to the predicted label (*Pred IC*), and misclassified trajectories with explanations extracted with respect to the true label (*True IC*). As shown in the tables, correctly classified trajectories yield concise and semantically coherent formulae. For misclassified instances, they tend to become substantially more complex and lengthy. This suggests that the model resorts to more elaborate temporal conditions when its internal representation is less confident or misaligned with the data, requiring more intricate rules to justify its decisions.

The postprocessing step, which refines formula thresholds and simplifies redundant logical structures, consistently reduces the average formula length while maintaining semantic integrity and discriminative power. As expected, the number of variables remains stable across pre- and postprocessing, since simplification only affects formula composition rather than the underlying signal dimensions. These results confirm the effectiveness of our rescaling and simplification procedures in enhancing readability without compromising explanation fidelity.

Global explanations, summarised in Table 5, follow similar patterns. Each table entry includes the global separability scores, as defined in Equation 7, filtered by correctly (*Sep C*) and incorrectly (*Sep IC*) classified trajectories, as well as for all trajectories combined (*Sep*), encompassing both correct and incorrect classifications. Moreover, we report the average number of syntactic nodes and variables of the global classifier before (*Readability Pre*) and after (*Readability Post*) postprocessing, summarising the overall compactness, indicated by the number of nodes, and dimensional coverage, indicated by number of variables, of the class-level formulae. Lastly, the table presents *Recall*, *Specificity* and *Precision* scores of the global explanation-based classifier. These metrics

Table 3. Readability statistics of local explanations before postprocessing. “C” denotes correctly classified samples; “*Pred IC*” and “*true IC*” refer to explanations constructed with respect to predicted and true labels of misclassified samples, respectively. “nodes” is the average number of syntactic operators per formula, and “vars” indicates the number of distinct variables used.

Dataset	C nodes	Pred IC nodes	True IC nodes	C vars	Pred IC vars	True IC vars
BasicMotions (BM)	9.55 ± 12.43	20.33 ± 13.20	14.67 ± 5.19	2.08 ± 1.35	4.00 ± 1.41	3.67 ± 0.94
ERing (ER)	4.07 ± 2.20	5.23 ± 2.54	5.18 ± 3.44	1.30 ± 0.49	1.59 ± 0.59	1.51 ± 0.55
Epilepsy (EP)	10.41 ± 10.89	12.00 ± 7.48	39.67 ± 35.12	1.58 ± 0.72	2.33 ± 0.94	2.00 ± 0.82

Table 4. Readability statistics of local explanations after postprocessing. Postprocessing consistently reduces syntactic length while preserving the relative complexity difference between correct and incorrect predictions.

Dataset	C nodes	Pred IC nodes	True IC nodes	C vars	Pred IC vars	True IC vars
BasicMotions (BM)	9.07 ± 11.25	19.00 ± 11.31	14.33 ± 4.71	2.08 ± 1.35	4.00 ± 1.41	3.67 ± 0.94
ERing (ER)	3.78 ± 2.16	4.74 ± 2.32	4.69 ± 3.01	1.30 ± 0.49	1.59 ± 0.59	1.51 ± 0.55
Epilepsy (EP)	9.20 ± 9.71	9.67 ± 6.18	34.00 ± 31.95	1.58 ± 0.72	2.33 ± 0.94	2.00 ± 0.82

Table 5. Global explanation separability and readability. “Sep” corresponds to global separability (as defined in Equation 7) computed on correctly classified (C), misclassified (IC), or all samples. “Readability” reports the mean \pm standard deviation of syntactic nodes (n) and variables (v). “Spec” is specificity, “Prec” is precision.

Dataset	Sep C (%)	Sep IC (%)	Sep (%)	Readability Pre	Readability Post	Recall	Spec	Prec
BasicMotions (BM)	59.9%	76.4%	60.6%	$46.2 \pm 42.8n, 3.0 \pm 2.1v$	$30.2 \pm 26.8n, 3.0 \pm 2.1v$	50.0%	97.5%	87.0%
ERing (ER)	74.5%	40.9%	71.4%	$8.7 \pm 3.2n, 2.0 \pm 0.6v$	$8.7 \pm 3.2n, 2.0 \pm 0.6v$	66.7%	98.7%	98.9%
Epilepsy (EP)	72.2%	95.9%	71.8%	$106.0 \pm 53.8n, 3.0 \pm 0.0v$	$101.8 \pm 52.0n, 3.0 \pm 0.0v$	74.6%	93.9%	80.5%

measure the extent to which the extracted logical rules successfully replicate the neural network’s classification performance, providing insight into whether the explanations capture the essential decision boundaries learned by the neural network.

The global separability scores remain relatively high across datasets, confirming that the selected logical formulae effectively capture discriminative temporal patterns.

Interestingly, separability scores for incorrectly classified (IC) cases are most times higher than for correct ones, though these explanations tend to be substantially more complex, as reflected in their higher node counts. This suggests that the model continues to identify discriminative patterns in misclassified cases, but expresses them through more complex logical formulae, which are consequently more difficult to interpret. Readability analysis further shows that postprocessing effectively reduces formula length while maintaining a stable number of variables across all conditions. Finally, the global recall, specificity, and precision values indicate that class-level explanations are both selective and faithful to the model’s decision boundaries: high specificity confirms that global concepts rarely activate for unrelated classes, while moderate recall and precision reflect a balanced coverage of relevant temporal features without overfitting to class noise. Together, these results demonstrate that STELLE’s local and global explanations remain discriminative, interpretable, and consistent with model behaviour across domains. The combination of symbolic interpretability and practical efficiency reinforces its potential as a trustworthy neuro-symbolic framework for time series classification.

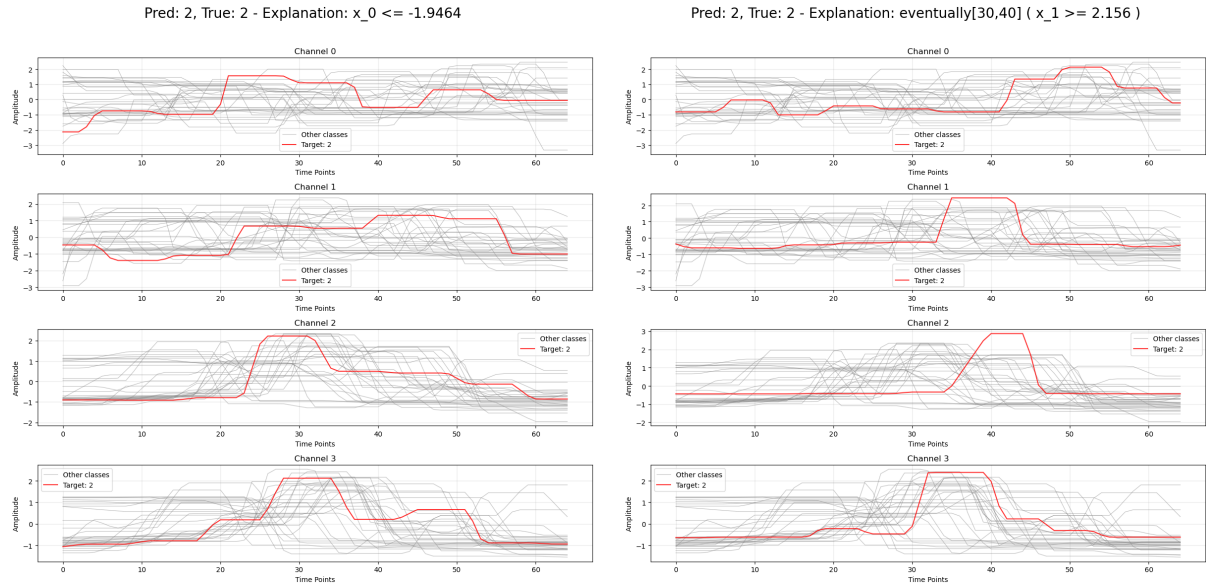


Fig. 2. Local explanations for two trajectories in the *ERing* dataset, showing the target trajectory (in red) and the trajectories from other classes (in gray) across its four channels. As title, the true and predicted class, and the proposed postprocessed explanation.

Computation times vary substantially across datasets but remain practical, with inference consistently completing in under one minute and full training with explanation extraction never exceeding one hour on the above-mentioned setup. Overall, these results demonstrate that STELLE produces concise, fully separable, and computationally tractable logical explanations, bridging symbolic reasoning with time series classification.

As a practical example, we report in Figure 2 and Figure 3 a subset of local explanations and the global explanations, respectively, generated for the dataset *ERing*, which contains 6 classes and 4 variables. The local explanations (Figure 2) showcase STELLE’s ability to identify instance-specific temporal patterns that drive classification decisions. The explanations are expressed as STL formulae with temporal operators and threshold conditions on specific features:

$$\begin{aligned} &x_0 \leq -1.9464 \\ &\mathbf{F}_{[30,40]} (x_1 \geq 2.156) \end{aligned}$$

This provides human-readable rules in the form of natural language-like statements that are accessible to all, regardless of their technical background or domain expertise.

The visualisations provide evidence of the explanations’ validity: the red highlighted time series, the targets, clearly exhibit the patterns described in the explanations. In the first instance, feature x_0 remains below the threshold throughout the early time window, while in the second instance, feature x_1 spikes above 2.156 in the time window [30, 40], exactly as specified by the *Eventually* operator.

The global explanation (Figure 3) provides a class-level understanding for class 2 that generalises across multiple instances of the same class shown in the local explanations. The formula reveals three distinct temporal

pathways through which a time series can be classified as class 2, which can be interpreted as

$$\begin{aligned} & F_{[12,19]} (x_1 \geq 1.8418) \\ & F_{[12,19]} (x_1 \geq 1.8418) \text{ and } (G_{[29,38]} (x_2 \leq -0.33) \\ & G_{[20,22]} (F_{[3,33]} (x_3 \leq -0.0514) \text{ and } x_3 \geq 1.5653)) \end{aligned}$$

These conditions, connected by logical OR operators, indicate that a time series belongs to class 2 if it satisfies at least one of these three temporal patterns.

This disjunctive structure demonstrates STELLE's ability to capture the diverse temporal patterns that characterise a single class. The multiple trajectories visible in red show how different instances of class 2 can satisfy different parts of the global formula while still belonging to the same class. This flexibility is crucial for capturing the natural variability present in real-world time series data.

These results demonstrate STELLE's dual contribution to explainable time series classification. First, local explanations allow to verify individual predictions, enabling debugging and identification of potential errors or biases in specific instances. Second, global explanations reveal temporal patterns at the class level, potentially uncovering domain insights about the underlying processes generating the time series.

6 Related work

Explainable AI (XAI) for TSC. TSC involves learning a classifier which associates trajectories with a probability distribution over discrete class labels. It is a traditional problem in ML (Bagnall, Lines, et al. 2016; Ruiz et al. 2021) with DL approaches being the state of the art in this field (Fawaz et al. 2018). Among them generative models are becoming popular for TSC, recently being enriched by foundation models for time series data (Liang et al. 2024), built on top of the Transformer architecture (Vaswani et al. 2023), to learn versatile representations of trajectories from vast amounts of data. XAI in the TSC context mostly adapts techniques from other domains to time series (Theissler et al. 2022; Turbé et al. 2023). Recent surveys (Arsenault et al. 2025; Rojat et al. 2021; Šimić et al. 2021) underscore the growing need for time-series-specific explainability, especially in high-risk domains. Toolkit developments such as Tsinterpret (Höllig et al. 2022) and evaluations of perturbation robustness (Schlegel and Keim 2023) highlight practical and reliability challenges in time series XAI. Attribution methods are arguably the most prominent techniques, aiming to identify time points or sub-sequences in the input that most influenced the prediction. Attention-based explanations, for instance, leverage attention mechanisms (Ge et al. 2018; Karim et al. 2018; Vinayavekhin et al. 2018) to assign relevance scores to parts of the sequence. Extensions of this idea to multivariate settings include models that simultaneously learn to attend to both important time intervals and variables (Hsieh et al. 2020), or dual-mode architectures designed for interpretability across feature and temporal dimensions (Cai et al. 2024).

Beyond temporal attribution, several works have proposed alternative interpretability strategies. Some focus on learning inherently interpretable representations of trajectories, such as the prototype-based latent space introduced in Baldán and Benítez (2021). Others explore post-hoc or counterfactual explanations: (Refoyo and Luengo 2024) proposes sparse, subsequence-based counterfactuals that highlight minimal changes needed to alter the prediction, while ensemble-based approaches have been used to identify robust, medically-relevant features driving predictions in multivariate time series (Metsch et al. 2025). Functional decomposition (Graaff et al. 2024) offers a novel route to interpretable feature-level explanations by aligning latent behaviour with meaningful subsequence dynamics. Symbolic approaches such as EMeriTAtE+DF (Bergami et al. 2025) show that hybrid numeric-event reasoning can improve both verifiability and explainability in multivariate settings. While EMeriTAtE+DF generates explanations through hybrid numeric-event detection (e.g., identifying statistical anomalies as events), STELLE advances this paradigm by fully grounding explanations in temporal logic semantics,

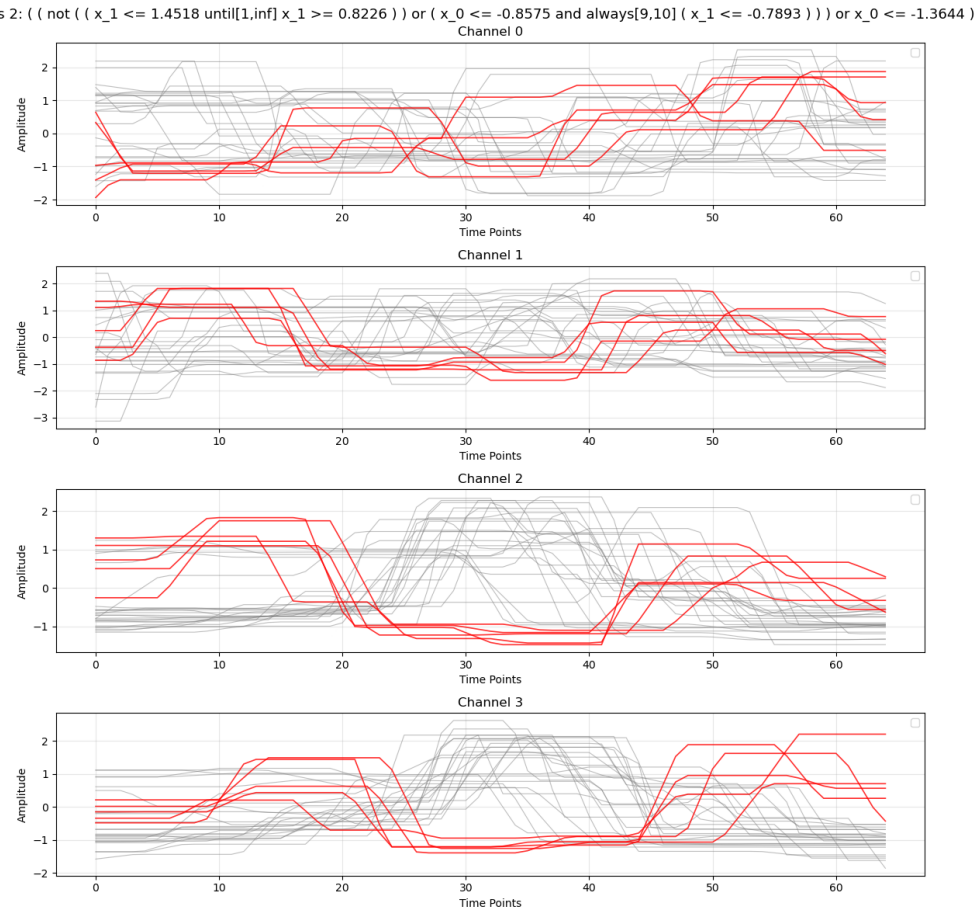


Fig. 3. Global explanation for class 2 in the *ERing* dataset, showing the target trajectories (in red) taken from the test set wrt their predicted class, and the training trajectories from other classes (in gray) across its four channels. As title, the class and the proposed postprocessed explanation.

representing concepts as STL formulae that explicitly encode temporal relationships and enabling direct logical verification of model decisions.

Learning temporal logic formulae as TS classifiers. Learning temporal logic formulae as TS classifiers has recently received notable attention. Pioneer works (Bombara et al. 2016; Mohammadinejad et al. 2020; Nenzi et al. 2018) cast the TSC problem as a data-driven requirement mining task, and use the evaluation of the mined properties as classifier. Related symbolic approaches, such as those by Kadous (1970), have historically explored parameterised event primitives to extract global, rule-based classifiers from time series data, anticipating more recent developments in symbolic temporal reasoning. More recently NeSy models have emerged in this context, which can be roughly divided in: (i) methods combining a decision tree approach for TSC, in which nodes of the tree represent STL formulae, where either activation functions mimic robust semantics, or time series features are extracted using Neural Networks (NN) to decide how to split the tree nodes (Pagliarini et al. 2024; Yan, Ma,

et al. 2022); and (ii) works directly translating the syntax tree of a temporal formulae into a NN, with neurons corresponding to different operators, and activation functions specifically devised towards solving TSC (Li et al. 2024; Yan, Julius, et al. 2021). In all these works however, the learned temporal formulae represent global, i.e. class-wise, explanations, as opposed to STELLE which natively computes local explanations, from which global ones can be naturally inferred. Our model evaluates a fixed set of human-interpretable STL formulae directly on the input trajectories. This direct, concept-based embedding allows explanation to be decoupled from fixed prototypes or latent structures, promoting diversity in the explanations while keeping them concise and logically grounded.

Concept-based models for TS data. Concept-based models for TS data did not receive much attention, with some notable exceptions: concepts extracted by clustering raw time series and possibly combined with domain knowledge are used in Jastrzebska et al. (2021) for TSC and data analysis; prototypes, which are class-representative trajectories, have also been widely used in TSC to facilitate the identification of patterns and improve the interpretability of classification models (Ghosal and Abbasi-Asl 2021; Obermair et al. 2022; Wang et al. 2025); the concept activation vector approach (Kim et al. 2017) has instead been recast for TSC in Asadi et al. (2022), by using human-defined concepts. Some works also explore symbolic abstraction via interpretable rule sets or logical primitives (e.g., Kadous (1970)), but these typically rely on handcrafted features or predefined event templates, lacking the data-driven adaptability of concept-based neural models. Hence, to the best of our knowledge, ours is the first approach proposing a NeSy concept-based architecture for TSC, in which temporal logic concepts are automatically inferred without human intervention.

Learning meaningful vector representations of TS. is a longstanding goal in machine learning. Classical approaches, such as dynamic time warping (DTW) combined with dimensionality reduction techniques (Mizuhara et al. 2006), and shapelet-based methods (Bostrom and Bagnall 2017; Ye and Keogh 2009) offer interpretable yet limited representations. More recent deep learning techniques like TS2Vec (Yue et al. 2022) and LETS-C (Kaur et al. 2024) learn embeddings via contrastive or language-inspired mechanisms, focusing on predictive performance over interpretability. Recent work in self-explainable graph-based models (García-Sigüenza et al. 2025) and verbalised spatio-temporal explanations (Spolaor 2023) suggests a shift towards integrating explainability into the architecture itself.

7 Conclusions

We introduced a novel interpretable framework for time series classification that leverages concepts expressed in Signal Temporal Logic (STL) and embeds both input trajectories and logical formulae into a shared semantic space. By designing a robustness-based kernel for input trajectories, we enable a direct and interpretable mapping from raw time series to symbolic representations, ensuring consistency between the classification mechanism and its logical explanations.

Our neuro-symbolic architecture combines the expressive power of temporal logic with the flexibility of neural modelling, allowing predictions to be explained through human-understandable temporal relations. Explanations are extracted both locally, for individual predictions, and globally, as class-characterising logical formulae obtained through symbolic aggregation. This integration ensures that interpretability is intrinsic to the model design, rather than an external post hoc component.

Our experimental evaluation on a diverse set of multivariate time series benchmarks demonstrates that STELLE achieves competitive predictive performance compared to state-of-the-art black-box models, while uniquely providing symbolic explanations grounded in Signal Temporal Logic. Although it does not consistently rank

among the top-performing methods in accuracy, STELLE maintains stable results across domains and offers a level of interpretability unattainable by existing neural or ensemble-based approaches.

Future Work. Future developments will focus on improving the framework's scalability and adaptability. We plan to reduce the computational overhead of concept generation through more efficient sampling and optimization techniques, enabling efficient reasoning with high-dimensional or long-horizon data. One promising direction is to extend STELLE with hierarchical or probabilistic temporal logics, which could enhance its expressivity while preserving interpretability. Furthermore, incorporating online and continual learning mechanisms would allow the provided explanations to evolve with non-stationary data, supporting long-term deployment in dynamic domains.

Societal implications. STELLE's interpretable logic-based explanations can enhance trust in safety-critical applications like medical diagnostics or autonomous systems, while reducing risks of black-box bias. However, simplified logical representations may overlook complex temporal patterns, requiring careful validation to prevent misinterpretation in high-stakes decisions.

Limitations. While the proposed framework demonstrates strong performance and interpretability across diverse time series classification tasks, several limitations remain. First, the generation and evaluation of large numbers of candidate STL formulae introduce a significant computational overhead during concept construction. This step scales with both the number of variables and the density of the parameter grid, which may limit applicability to very high-dimensional or long-horizon datasets. Second, the model's interpretability depends on the comprehensibility of individual formulae. Although we constrain formula depth and variable count during the construction of atomic temporal patterns, the process of combining multiple formulae with different variables to generate local and global explanations can result in complex composite expressions where both the variable count and formula length increase substantially, potentially reaching a level of complexity that becomes difficult for humans to interpret and understand.

Acknowledgments

This study was carried out within the PNRR research activities of the consortium iNEST (Interconnected North-East Innovation Ecosystem) funded by the European Union NextGenerationEU (Piano Nazionale di Ripresa e Resilienza (PNRR) Missione 4 Componente 2, Investimento 1.5 D.D. 1058 23062022, ECS_00000043). This manuscript reflects only the Authors' views and opinions, neither the European Union nor the European Commission can be considered responsible for them.

References

P.-D. Arsenault, S. Wang, and J.-M. Patenaude. May 2025. "A Survey of Explainable Artificial Intelligence (XAI) in Financial Time Series Forecasting." *ACM Computing Surveys*, 57, 10, (May 2025), 1–37. doi:[10.1145/3729531](https://doi.org/10.1145/3729531).

M. Asadi, V. Swamy, J. Frej, J. T. T. Vignoud, M. Marras, and T. Käser. 2022. "Ripple: Concept-Based Interpretation for Raw Time Series Models in Education." In: *AAAI Conference on Artificial Intelligence*.

E. Asarin, A. Donzé, O. Maler, and D. Nickovic. 2011. "Parametric Identification of Temporal Properties." In: *Runtime Verification - Second International Conference, RV 2011, Revised Selected Papers* (Lecture Notes in Computer Science). Vol. 7186. Springer, 147–160.

A. Bagnall, J. Lines, A. G. Bostrom, J. Large, and E. J. Keogh. 2016. "The great time series classification bake off: a review and experimental evaluation of recent algorithmic advances." *Data Mining and Knowledge Discovery*, 31, 606–660.

A. Bagnall, H. A. Dau, J. Lines, M. Flynn, J. Large, A. Bostrom, P. Southam, and E. Keogh. 2018. *The UEA multivariate time series classification archive, 2018*. (2018). arXiv: [1811.00075 \(cs.LG\)](https://arxiv.org/abs/1811.00075).

A. Bagnall, M. Flynn, J. Large, J. Lines, and M. Middlehurst. 2020. *On the Usage and Performance of the Hierarchical Vote Collective of Transformation-Based Ensembles Version 1.0 (HIVE-COTE v1.0)*. Springer International Publishing, 3–18. ISBN: 9783030657420. doi:[10.1007/978-3-030-65742-0_1](https://doi.org/10.1007/978-3-030-65742-0_1).

F. J. Baldán and J. M. Benítez. 2021. "Multivariate times series classification through an interpretable representation." *Information Sciences*, 569, 596–614. doi:<https://doi.org/10.1016/j.ins.2021.05.024>.

E. Bartocci, J. V. Deshmukh, A. Donzé, G. Fainekos, O. Maler, D. Nickovic, and S. Sankaranarayanan. 2018. "Specification-Based Monitoring of Cyber-Physical Systems: A Survey on Theory, Tools and Applications." In: *Lectures on Runtime Verification - Introductory and Advanced Topics*. Lecture Notes in Computer Science. Vol. 10457. Springer, 135–175.

E. Bartocci, C. Mateis, E. Nesterini, and D. Nickovic. 2022. "Survey on mining signal temporal logic specifications." *Inf. Comput.*, 289, Part, 104957.

G. Bergami, E. Packer, K. Scott, and S. D. Din. 2025. *Towards Explainable Sequential Learning*. (2025). arXiv: [2505.23624 \(cs.DB\)](https://arxiv.org/abs/2505.23624).

G. Bombara, C.-I. Vasile, F. Penedo, H. Yasuoka, and C. Belta. 2016. "A Decision Tree Approach to Data Classification using Signal Temporal Logic." In: *Proceedings of the 19th International Conference on Hybrid Systems: Computation and Control (HSCC '16)*. Association for Computing Machinery, Vienna, Austria, 1–10. ISBN: 9781450339551. doi:[10.1145/2883817.2883843](https://doi.org/10.1145/2883817.2883843).

L. Bortolussi, G. M. Gallo, J. Kretínský, and L. Nenzi. 2022. "Learning Model Checking and the Kernel Trick for Signal Temporal Logic on Stochastic Processes." In: *Tools and Algorithms for the Construction and Analysis of Systems - 28th International Conference, TACAS 2022, Proceedings, Part I*.

A. Bostrom and A. Bagnall. July 2017. *Binary Shapelet Transform for Multiclass Time Series Classification*. (July 2017), 24–46. ISBN: 978-3-662-55607-8. doi:[10.1007/978-3-662-55608-5_2](https://doi.org/10.1007/978-3-662-55608-5_2).

W. Cai, X. Zhu, K. Bai, A. Ye, and R. Zhang. 2024. "An explainable dual-mode convolutional neural network for multivariate time series classification." *Knowledge-Based Systems*, 299, 112015. doi:<https://doi.org/10.1016/j.knosys.2024.112015>.

S. Daulton, M. Balandat, and E. Bakshy. 2021. *Parallel Bayesian Optimization of Multiple Noisy Objectives with Expected Hypervolume Improvement*. (2021). <https://arxiv.org/abs/2105.08195> arXiv: [2105.08195 \(cs.LG\)](https://arxiv.org/abs/2105.08195).

A. Dempster, F. Petitjean, and G. I. Webb. 2020. "ROCKET: Exceptionally Fast and Accurate Time Series Classification Using Random Convolutional Kernels." *Data Mining and Knowledge Discovery*, 34, 5, 1454–1495.

H. Deng, G. Runger, E. Tuv, and M. Vladimir. 2013. *A Time Series Forest for Classification and Feature Extraction*. (2013). arXiv: [1302.2277 \(cs.LG\)](https://arxiv.org/abs/1302.2277).

A. Donzé, T. Ferrère, and O. Maler. July 2013. "Efficient Robust Monitoring for STL." In: vol. 8044. (July 2013). ISBN: 978-3-642-39798-1. doi:[10.1007/978-3-642-39799-8_19](https://doi.org/10.1007/978-3-642-39799-8_19).

European Commission. 2016. *Regulation (EU) 2016/679 of the European Parliament and of the Council of 27 April 2016 on the protection of natural persons with regard to the processing of personal data and on the free movement of such data, and repealing Directive 95/46/EC (General Data Protection Regulation) (Text with EEA relevance)*. (2016).

H. I. Fawaz, G. Forestier, J. Weber, L. Idoumghar, and P.-A. Muller. 2018. "Deep learning for time series classification: a review." *Data Mining and Knowledge Discovery*, 33, 917–963.

J. García-Sigüenza, M. Curado, F. Llorens-Largo, and J. F. Vicent. 2025. "Self explainable graph convolutional recurrent network for spatio-temporal forecasting." *Machine Learning*, 114, 1, 2.

W. Ge, J.-W. Huh, Y. R. Park, J.-H. Lee, Y.-H. Kim, and A. Turchin. 2018. "An Interpretable ICU Mortality Prediction Model Based on Logistic Regression and Recurrent Neural Networks with LSTM units." In: *AMIA Annual Symposium Proceedings*. Vol. 2018. American Medical Informatics Association, 460.

A. Ghorbani, J. Wexler, J. Zou, and B. Kim. 2019. *Towards Automatic Concept-based Explanations*. (2019). arXiv: [1902.03129 \(stat.ML\)](https://arxiv.org/abs/1902.03129).

G. R. Ghosal and R. Abbasi-Asl. 2021. *Multi-Modal Prototype Learning for Interpretable Multivariable Time Series Classification*. (2021). arXiv: [2106.09636 \(cs.LG\)](https://arxiv.org/abs/2106.09636).

T. de Graaff, M. Wild, T. Werner, E. Möhlmann, S. Seibt, and B. Ebrecht. 2024. "Increasing Explainability in Time Series Classification by Functional Decomposition." In: *Explainable Artificial Intelligence*. Ed. by L. Longo, S. Lapuschkin, and C. Seifert. Springer Nature Switzerland, Cham, 125–144.

C. R. Harris et al. Sept. 2020. "Array programming with NumPy." *Nature*, 585, 7825, (Sept. 2020), 357–362. doi:[10.1038/s41586-020-2649-2](https://doi.org/10.1038/s41586-020-2649-2).

D. Helbing. 2019. *Societal, Economic, Ethical and Legal Challenges of the Digital Revolution: From Big Data to Deep Learning, Artificial Intelligence, and Manipulative Technologies*. Ed. by D. Helbing. Springer International Publishing, Cham, 47–72. ISBN: 978-3-319-90869-4. doi:[10.1007/978-3-319-90869-4_6](https://doi.org/10.1007/978-3-319-90869-4_6).

J. Hills, J. Lines, E. Baranauskas, J. Mapp, and A. Bagnall. July 2014. "Classification of time series by shapelet transformation." *Data Mining and Knowledge Discovery*, 28, 4, (July 2014), 851–881. doi:[10.1007/s10618-013-0322-1](https://doi.org/10.1007/s10618-013-0322-1).

A. Ho. Feb. 2019. "Deep Ethical Learning: Taking the Interplay of Human and Artificial Intelligence Seriously." *The Hastings Center report*, 49, (Feb. 2019), 36–39. doi:[10.1002/hast.977](https://doi.org/10.1002/hast.977).

J. Höllig, C. Kulbach, and S. Thoma. 2022. *TSInterpret: A unified framework for time series interpretability*. (2022). arXiv: [2208.05280 \(cs.LG\)](https://arxiv.org/abs/2208.05280).

T.-Y. Hsieh, S. Wang, Y. Sun, and V. Honavar. 2020. *Explainable Multivariate Time Series Classification: A Deep Neural Network Which Learns To Attend To Important Variables As Well As Informative Time Intervals*. (2020). arXiv: [2011.11631 \(cs.LG\)](https://arxiv.org/abs/2011.11631).

M. Iman, H. R. Arabnia, and R. M. Branchinst. 2021. "Pathways to Artificial General Intelligence: A Brief Overview of Developments and Ethical Issues via Artificial Intelligence, Machine Learning, Deep Learning, and Data Science." In: *Advances in Artificial Intelligence and*

Applied Cognitive Computing. Ed. by H. R. Arabnia, K. Ferens, D. de la Fuente, E. B. Kozerenko, J. A. Olivas Varela, and F. G. Tinetti. Springer International Publishing, Cham, 73–87. ISBN: 978-3-030-70296-0.

H. Ismail Fawaz et al. Sept. 2020. “InceptionTime: finding AlexNet for time series classification.” English. *Data Mining and Knowledge Discovery*, 34, (Sept. 2020), 1936–1962. doi:[10.1007/s10618-020-00710-y](https://doi.org/10.1007/s10618-020-00710-y).

A. M. Jastrzebska, G. Nápoles, Y. Salgueiro, and K. Vanhoof. 2021. “Evaluating time series similarity using concept-based models.” *Knowl. Based Syst.*, 238, 107811.

M. Kadous. Feb. 1970. “Learning Comprehensible Descriptions of Multivariate Time Series.” (Feb. 1970).

F. Karim, S. Majumdar, H. Darabi, and S. Chen. 2018. “LSTM Fully Convolutional Networks for Time Series Classification.” *IEEE Access*, 6, 1662–1669. doi:[10.1109/access.2017.2779939](https://doi.org/10.1109/access.2017.2779939).

I. Karlsson, P. Papapetrou, and H. Boström. Sept. 2016. “Generalized random shapelet forests.” *Data Mining and Knowledge Discovery*, 30, (Sept. 2016). doi:[10.1007/s10618-016-0473-y](https://doi.org/10.1007/s10618-016-0473-y).

R. Kaur, Z. Zeng, T. Balch, and M. Veloso. 2024. *LETS-C: Leveraging Language Embedding for Time Series Classification*. (2024). arXiv: [2407.06533 \(cs.LG\)](https://arxiv.org/abs/2407.06533).

B. Kim, M. Wattenberg, J. Gilmer, C. J. Cai, J. Wexler, F. B. Viégas, and R. Sayres. 2017. “Interpretability Beyond Feature Attribution: Quantitative Testing with Concept Activation Vectors (TCAV).” In: *International Conference on Machine Learning*.

B. Leichtmann, C. Humer, A. Hinterreiter, M. Streit, and M. Mara. 2023. “Effects of Explainable Artificial Intelligence on trust and human behavior in a high-risk decision task.” *Computers in Human Behavior*, 139, 107539. doi:<https://doi.org/10.1016/j.chb.2022.107539>.

D. Li, M. Cai, C.-I. Vasile, and R. Tron. 2024. *TLINet: Differentiable Neural Network Temporal Logic Inference*. (2024). arXiv: [2405.06670 \(cs.LO\)](https://arxiv.org/abs/2405.06670).

Y. Liang, H. Wen, Y. Nie, Y. Jiang, M. Jin, D. Song, S. Pan, and Q. Wen. 2024. “Foundation Models for Time Series Analysis: A Tutorial and Survey.” *ArXiv*, abs/2403.14735.

O. Maler and D. Nickovic. Jan. 2004. “Monitoring Temporal Properties of Continuous Signals.” In: vol. 3253. (Jan. 2004), 152–166. ISBN: 978-3-540-23167-7. doi:[10.1007/978-3-540-30206-3_12](https://doi.org/10.1007/978-3-540-30206-3_12).

J. M. Metsch, P. Hempel, M. C. Maurer, N. Spicher, and A.-C. Hauschild. 2025. “Ensemble Post-hoc Explainable AI in Multivariate Time Series: Identifying Medical Features Driving Disease Prediction.” *bioRxiv*. eprint: <https://www.biorxiv.org/content/early/2025/02/18/2025.02.14.638219.full.pdf>. doi:[10.1101/2025.02.14.638219](https://doi.org/10.1101/2025.02.14.638219).

M. Middlehurst, A. Ismail-Fawaz, et al. 2024. “aeon: a Python Toolkit for Learning from Time Series.” *Journal of Machine Learning Research*, 25, 289, 1–10.

M. Middlehurst, J. Large, and A. Bagnall. Dec. 2020. “The Canonical Interval Forest (CIF) Classifier for Time Series Classification.” In: *2020 IEEE International Conference on Big Data (Big Data)*. IEEE, (Dec. 2020), 188–195. doi:[10.1109/bigdata50022.2020.9378424](https://doi.org/10.1109/bigdata50022.2020.9378424).

M. Middlehurst, J. Large, G. Cawley, and A. Bagnall. 2021. *The Temporal Dictionary Ensemble (TDE) Classifier for Time Series Classification*. Springer International Publishing, 660–676. ISBN: 9783030676582. doi:[10.1007/978-3-030-67658-2_38](https://doi.org/10.1007/978-3-030-67658-2_38).

M. Middlehurst, J. Large, M. Flynn, J. Lines, A. Bostrom, and A. Bagnall. Sept. 2021. “HIVE-COTE 2.0: a new meta ensemble for time series classification.” *Machine Learning*, 110, 11–12, (Sept. 2021), 3211–3243. doi:[10.1007/s10994-021-06057-9](https://doi.org/10.1007/s10994-021-06057-9).

M. Middlehurst, W. Vickers, and A. Bagnall. 2019. “Scalable Dictionary Classifiers for Time Series Classification.” In: *Intelligent Data Engineering and Automated Learning – IDEAL 2019: 20th International Conference, Manchester, UK, November 14–16, 2019, Proceedings, Part I*. Springer-Verlag, Manchester, United Kingdom, 11–19. ISBN: 978-3-030-33606-6. doi:[10.1007/978-3-030-33607-3_2](https://doi.org/10.1007/978-3-030-33607-3_2).

S. Mitchell, M. O’Sullivan, and I. Dunning. 2011. “PuLP : A Linear Programming Toolkit for Python.” In.

Y. Mizuhara, A. Hayashi, and N. Suematsu. 2006. “Embedding of time series data by using dynamic time warping distances.” *Systems and Computers in Japan*, 37, 3, 1–9. eprint: <https://onlinelibrary.wiley.com/doi/pdf/10.1002/scj.20486>. doi:<https://doi.org/10.1002/scj.20486>.

S. Mohammadinejad, J. V. Deshmukh, A. G. Puranic, M. Vazquez-Chanlatte, and A. Donzé. 2020. “Interpretable classification of time-series data using efficient enumerative techniques.” In: *HSCC ’20: 23rd ACM International Conference on Hybrid Systems: Computation and Control*. ACM, 9:1–9:10.

L. Nenzi, S. Silvetti, E. Bartocci, and L. Bortolussi. 2018. “A Robust Genetic Algorithm for Learning Temporal Specifications from Data.” In: *Quantitative Evaluation of Systems - 15th International Conference, Beijing, China, Proceedings* (Lecture Notes in Computer Science). Vol. 11024. Springer, 323–338.

T. Nguyen, S. Gspaner, I. Ilie, M. O’reilly, and G. Ifrim. July 2019. “Interpretable time series classification using linear models and multi-resolution multi-domain symbolic representations.” *Data Min. Knowl. Discov.*, 33, 4, (July 2019), 1183–1222. doi:[10.1007/s10618-019-00633-3](https://doi.org/10.1007/s10618-019-00633-3).

C. Obermair, A. Fuchs, F. Pernkopf, L. Felsberger, A. Apollonio, and D. Wollmann. 2022. “Example or Prototype? Learning Concept-Based Explanations in Time-Series.” In: *Asian Conference on Machine Learning*.

M. Olson et al. 2025. “Ax: A Platform for Adaptive Experimentation.” In: *AutoML 2025 ABCD Track*.

G. Pagliarini, S. Scaboro, G. Serra, G. Sciaovicco, and E. I. Stan. 2024. “Neural-Symbolic Temporal Decision Trees for Multivariate Time Series Classification.” In: *Time*.

A. Paszke et al. 2019. *PyTorch: an imperative style, high-performance deep learning library*. Curran Associates Inc., Red Hook, NY, USA, 12 pages.

F. Pedregosa et al. 2011. “Scikit-learn: Machine Learning in Python.” *Journal of Machine Learning Research*, 12, 2825–2830.

A. Pnueli. 1977. "The temporal logic of programs." In: *18th Annual Symposium on Foundations of Computer Science (sfcs 1977)*, 46–57.

M. Refoyo and D. Luengo. 2024. *Multi-SpaCE: Multi-Objective Subsequence-based Sparse Counterfactual Explanations for Multivariate Time Series Classification*. (2024). arXiv: [2501.04009 \(cs.NE\)](https://arxiv.org/abs/2501.04009).

T. Rojat, R. Puget, D. Filliat, J. D. Ser, R. Gelin, and N. Díaz-Rodríguez. 2021. *Explainable Artificial Intelligence (XAI) on TimeSeries Data: A Survey*. (2021). arXiv: [2104.00950 \(cs.LG\)](https://arxiv.org/abs/2104.00950).

A. P. Ruiz, M. Flynn, J. Large, M. Middlehurst, and A. Bagnall. Dec. 2021. "The great multivariate time series Classification bake off: A review and experimental evaluation of recent algorithmic advances." *Data Mining and Knowledge Discovery*, 35, 2, (Dec. 2021), 401–449. doi:[10.1007/s10618-020-00727-3](https://doi.org/10.1007/s10618-020-00727-3).

G. Saveri and L. Bortolussi. 2024. "Retrieval-Augmented Mining of Temporal Logic Specifications from Data." In: *Machine Learning and Knowledge Discovery in Databases. Research Track*. Ed. by A. Bifet, J. Davis, T. Krilavičius, M. Kull, E. Ntoutsi, and I. Žliobaitė. Springer Nature Switzerland, Cham, 315–331. ISBN: 978-3-031-70368-3.

G. Saveri, L. Nenzi, L. Bortolussi, and J. Křetinský. 2024. *stl2vec: Semantic and Interpretable Vector Representation of Temporal Logic*. (2024). <https://arxiv.org/abs/2405.14389> arXiv: [2405.14389 \(cs.AI\)](https://arxiv.org/abs/2405.14389).

P. Schäfer and U. Leser. 2018. *Multivariate Time Series Classification with WEASEL+MUSE*. (2018). <https://arxiv.org/abs/1711.11343> arXiv: [1711.11343 \(cs.LG\)](https://arxiv.org/abs/1711.11343).

U. Schlegel and D. A. Keim. 2023. "A Deep Dive into Perturbations as Evaluation Technique for Time Series XAI." arXiv: [2307.05104 \(cs.LG\)](https://arxiv.org/abs/2307.05104).

I. Šimić, V. Sabol, and E. Veas. 2021. *XAI Methods for Neural Time Series Classification: A Brief Review*. (2021). arXiv: [2108.08009 \(cs.LG\)](https://arxiv.org/abs/2108.08009).

R. Spolaor. 2023. "Verbal Explanations of Spatio-Temporal Graph Neural Networks for Traffic Forecasting."

M. Sundararajan, A. Taly, and Q. Yan. 2017. *Axiomatic Attribution for Deep Networks*. (2017). <https://arxiv.org/abs/1703.01365> arXiv: [1703.01365 \(cs.LG\)](https://arxiv.org/abs/1703.01365).

A. Theissler, F. Spinnato, U. Schlegel, and R. Guidotti. 2022. "Explainable AI for Time Series Classification: A Review, Taxonomy and Research Directions." *IEEE Access*, 10, 100700–100724.

H. Turbé, M. Bjelogrlic, C. Lovis, and G. Mengaldo. 2023. "Evaluation of post-hoc interpretability methods in time-series classification." *Nature Machine Intelligence*, 5, 250–260.

A. Vaswani, N. Shazeer, N. Parmar, J. Uszkoreit, L. Jones, A. N. Gomez, L. Kaiser, and I. Polosukhin. 2023. *Attention Is All You Need*. (2023). arXiv: [1706.03762 \(cs.CL\)](https://arxiv.org/abs/1706.03762).

P. Vinayavakhin, S. Chaudhury, A. Munawar, D. J. Agrawante, G. D. Magistris, D. Kimura, and R. Tachibana. 2018. *Focusing on What is Relevant: Time-Series Learning and Understanding using Attention*. (2018). arXiv: [1806.08523 \(cs.CV\)](https://arxiv.org/abs/1806.08523).

Y. Wang, J. Cai, H. Yang, C. Shi, M. Zhang, J. Wang, R. Zhang, and X. Zhao. 2025. "Interpretable deep classification of time series based on class discriminative prototype learning." *Intelligent Data Analysis*, 0, 0, 1088467X251319188. eprint: <https://doi.org/10.1177/1088467X251319188>. doi:[10.1177/1088467X251319188](https://doi.org/10.1177/1088467X251319188).

R. Yan, A. A. Julius, M. Chang, A. Fokoue, T. Ma, and R. A. Uceda-Sosa. 2021. "STONE: Signal Temporal Logic Neural Network for Time Series Classification." *2021 International Conference on Data Mining Workshops (ICDMW)*, 778–787.

R. Yan, T. Ma, A. Fokoue, M. Chang, and A. A. Julius. 2022. "Neuro-symbolic Models for Interpretable Time Series Classification using Temporal Logic Description." *2022 IEEE International Conference on Data Mining (ICDM)*, 618–627.

L. Ye and E. Keogh. 2009. "Time series shapelets: a new primitive for data mining." In: *Proceedings of the 15th ACM SIGKDD international conference on Knowledge discovery and data mining*. ACM, 947–956.

C.-K. Yeh, B. Kim, S. Arik, C.-L. Li, T. Pfister, and P. Ravikumar. 2020. "On Completeness-aware Concept-Based Explanations in Deep Neural Networks." In: *Advances in Neural Information Processing Systems*. Ed. by H. Larochelle, M. Ranzato, R. Hadsell, M. Balcan, and H. Lin. Vol. 33. Curran Associates, Inc., 20554–20565.

Z. Yue, Y. Wang, J. Duan, T. Yang, C. Huang, Y. Tong, and B. Xu. 2022. *TS2Vec: Towards Universal Representation of Time Series*. (2022). arXiv: [2106.10466 \(cs.LG\)](https://arxiv.org/abs/2106.10466).

X. Zhang, Y. Gao, J. Lin, and C.-T. Lu. Apr. 2020. "TapNet: Multivariate Time Series Classification with Attentional Prototypical Network." *Proceedings of the AAAI Conference on Artificial Intelligence*, 34, 04, (Apr. 2020), 6845–6852. doi:[10.1609/aaai.v34i04.6165](https://doi.org/10.1609/aaai.v34i04.6165).

Appendix

A Kernel evaluation

Two kernel functions that capture the similarity between STL formulae and between trajectories and formulae are defined respectively in Equation 1 and Equation 3. Being the space \mathcal{T} of trajectories infinite-dimensional, we should define a measure over it, for being able to evaluate the two equations via Monte Carlo approximation. For this reason we provide a sampling algorithm for such measure, denoted as μ_0 , detailed in Algorithm 1, which

operates on piecewise linear functions over the interval $[a, b]$ (which is a dense subset of the set of continuous functions over $I \subseteq \mathbb{R}_{\geq 0}$).

Algorithm 1 μ_0 for sampling a trajectory over the interval $[a, b]$

Require: $\Delta, a, b, m', m'', \sigma', \sigma'', q$

Ensure: τ

```

 $\tau_0 \sim \mathcal{N}(m', \sigma')$                                 ▷ sample the starting point
 $\tau(t_0) \leftarrow \tau_0$                                      ▷ sample the total variation
 $K \sim (\mathcal{N}(m'', \sigma''))^2$ 
 $y_1, \dots, y_{N-1} \sim \mathbb{U}([0, K])$ 
 $y_0 \leftarrow 0, y_n \leftarrow K$ 
orderAndRename( $y_0, \dots, y_n$ )                                ▷ now  $y_1 \leq y_2 \leq \dots \leq y_{N-1}$ 
 $s_0 \sim \text{Discr}(-1, 1)$ 
for  $i = 0$  to  $N - 1$  do                                ▷  $P(s = -1) = q$ 
     $s \leftarrow \text{Binomial}(q)$ 
     $s_{i+1} \leftarrow s_i \cdot s$ 
     $\tau(t_{i+1}) \leftarrow \tau(t_i) + s_{i+1}(y_{i+1} - y_i)$ 
end for

```

Default parameters are set as $a = 0, b = 100, \Delta = 1, m' = m'' = 0'', \sigma' = \sigma'' = 1, q = 0.1$. Intuitively, μ_0 makes *simple* trajectories more probable, considering total variation and number of changes in monotonicity as indicators of complexity of signals. Note that although the feature space $\mathbb{R}^{\mathcal{T}}$ into which ρ maps formulae is infinite-dimensional, in practice the kernel trick allows to circumvent this issue by mapping each formula to a vector of dimension equal to the number of formulae which are in the training set used to evaluate the kernel (Gram) matrix.

B Concept selection and embedding

To construct a flexible and interpretable vocabulary of temporal logic concepts, we generate a large collection of STL formulae through symbolic enumeration, exploiting Parametric Signal Temporal Logic (PSTL) (Asarin et al. 2011). PSTL is an extension of STL that parameterises both the time bounds in the temporal operators and the thresholds in inequality predicates. Given a PSTL template and a parameter configuration, an STL formula is induced by instantiating its free parameters with the provided values.

Formula templates are constructed by recursively applying logical and temporal operators up to a maximum of $M = 5$ syntactic nodes. In order to ensure human interpretability, we limit the number of signal dimensions used per formula to $N \in \{1, 2, 3\}$. We do not allow more dimensions since, in practice, STL formulae involving a large number of variables tend to be difficult to interpret and verify visually. We found that restricting $N = 1$ already yielded strong performance across all metrics, and we retained this setting for the final experiments.

We explored two different strategies for generating formulae across multiple variables. Suppose a dataset has 4 variables and $N = 1$ is fixed. One approach was to generate, for instance, 1000 formulae by selecting the formulae per variable independently. An alternative approach involved generating 250 generic formulae with a placeholder variable, then duplicating them across all variables in the dataset (e.g., $x > 3$ becomes $x_0 > 3, x_1 > 3, x_2 > 3, x_3 > 3$). Empirically, both strategies proved essentially equivalent in performance but we adopt

the second method as our default, as it promotes structural consistency across dimensions and simplifies the generation pipeline. We empirically found that allocating 500 concepts per variable offered a good trade-off between coverage and computational efficiency. A minimum threshold of 1000 concepts is enforced to ensure sufficient semantic diversity, even for low-dimensional datasets.

Each formula template φ is instantiated over a dense grid of parameter configurations $\mathcal{P} = \{p_1, \dots, p_{|\mathcal{P}|}\}$ to produce a large pool of fully specified formulae $\varphi(p)$. These are evaluated over a representative set of trajectories $\mathcal{T} = \{\tau_1, \dots, \tau_{|\mathcal{T}|}\}$ using the quantitative STL semantics, yielding a robustness matrix $S \in \mathbb{R}^{|\mathcal{P}| \times |\mathcal{T}|}$, with entries

$$S(i, j) = \rho(\varphi(p_i), \tau_j)$$

Each row of S is a robustness signature that characterises the behaviour of a formula across trajectories.

Concept selection proceeds incrementally: candidate formulae are sampled in batches and compared to the current concept set via cosine similarity between their robustness signatures. A formula is retained if its similarity to all previously selected concepts is below a fixed threshold $t \in (0, 1]$. The threshold t directly controls the trade-off between behavioural diversity and conceptual granularity: lower values enforce stricter separation, resulting in more distinct concepts at the cost of longer selection time, while higher values yield denser coverage of the formula space with faster computation. We selected $t = 0.99$ as a good trade-off between computational efficiency and conceptual diversity.

When multiple candidates exhibit high similarity to existing concepts, we apply a preference for syntactic simplicity, retaining the structurally minimal representative among them. This procedure continues until the desired number of formulae is selected. The final concept set provides a compact, semantically diverse, and interpretable basis for embedding, reasoning, and symbolic explanation.

Algorithm 2 Algorithm for generating STL formulae templates

```

Require:  $M, N$ 
Ensure: all_phis
    all_phis  $\leftarrow []$ 
    all_phis.append(generateAtomicPropositions())
    for  $2 \leq m \leq M$  do
        ▷ retrieve templates with  $m - 1$  nodes
        prev_phis  $\leftarrow$  getPhisGivenNodes( $m - 1$ )
        ▷  $F, G, \neg$ 
        unary_ops  $\leftarrow$  expandbyUnaryOperators(prev_phis)
        all_phis.append(unary_ops)
        ▷ all pairs  $(l, r) : l + r = m, l \leq r$ 
        l_list, r_list  $\leftarrow$  getPairsGivenSum( $m$ )
        for  $(l, r) \in [l\_list, r\_list]$  do
            l_phis  $\leftarrow$  getPhisGivenNodes( $l$ )
            r_phis  $\leftarrow$  getPhisGivenNodes( $r$ )
            ▷  $\wedge, \vee, U$ 
            binary_ops  $\leftarrow$  expandbyBinaryOperators(l_phis, r_phis)
            all_phis.append(binary_ops)
        end for
    end for

```

C Formulae manipulation

In this section, we describe the postprocessing techniques applied to STL formulae in order to improve their interpretability, discriminative power, and syntactic simplicity. These procedures operate either by modifying formula thresholds based on observed robustness values, or by rewriting the logical structure using standard equivalences. Together, they ensure that the extracted explanations are both semantically meaningful and syntactically concise.

C.1 Threshold shift

To ensure that selected STL formulae are interpretable and exhibit class-discriminative behaviour, we apply a postprocessing step based on robustness analysis. For each input trajectory and its associated STL formula, we evaluate the formula's robustness over trajectories from all classes. If the robustness of the input trajectory lies outside the range of robustness values for the other classes, i.e., the formula separates the target class, we rescale the formula's threshold by a factor derived from the target robustness and its closest counterpart from other classes, aiming to enhance the separation margin.

If, instead, the formula does not separate the target class, we adapt its decision boundary by analysing its robustness landscape across all classes. Specifically, for each formula, we compare its robustness on the target trajectory with the robustness values computed over trajectories of other classes. When the robustness distribution indicates that the formula fails to distinguish the target class, we shift its threshold toward the midpoint between the target robustness and the closest opposing robustness value, thereby maximising inter-class separation while preserving the original temporal structure. In both cases, to maintain semantic consistency, if the resulting robustness for the target trajectory becomes negative, the formula is logically negated. The final postprocessed formulae are then simplified to ensure readability and syntactic minimality.

This process is described in Algorithm 3.

We now formally justify this behaviour by proving the following proposition, which establishes the linearity of robustness with respect to uniform threshold shifts.

PREPOSITION. *By uniformly modifying the thresholds of the variables in an STL formula φ by a constant δ , this adjustment will shift the robustness values linearly by δ .*

PROOF. We now provide proof of this statement for all STL. By proving that the Preposition holds true for every Atom and STL operator, the proof comes naturally for more complex structures.

Step 1: Atomic Predicates

Consider the atomic predicate $\pi(\mathbf{x}) = (f_\pi(\mathbf{x}) \geq 0)$ and a trajectory τ .

Its robustness value is:

$$\rho(\pi, \tau, t) = f_\pi(\tau(t))$$

If we adjust the threshold by a constant δ , this corresponds to modifying the predicate to

$$\pi'(\mathbf{x}) = (f_\pi(\mathbf{x}) + \delta \geq 0) = (f_\pi(\mathbf{x}) \geq -\delta)$$

The new robustness value becomes:

$$\rho'(\pi, \tau, t) = f_\pi(\tau(t)) - \delta = \rho(\pi, \tau, t) - \delta$$

Thus, a uniform adjustment by δ decreases the robustness linearly by δ .

Step 2: Temporal operators

Next, let's consider the impact on more complex formulae built from atomic predicates.

Let's start from *Negation*, whose definition is:

$$\rho(\neg\varphi, \tau, t) = -\rho(\varphi, \tau, t)$$

The a uniform adjustment by δ results in:

$$\begin{aligned}\rho'(\neg\varphi, \tau, t) &= -(\rho(\varphi, \tau, t) - \delta) \\ &= -\rho(\varphi, \tau, t) + \delta \\ &= \rho(\neg\varphi, \tau, t) + \delta\end{aligned}$$

This shows that the robustness shifts linearly by δ .

For *Conjunction*, defined as

$$\rho(\varphi_1 \wedge \varphi_2, \tau, t) = \min(\rho(\varphi_1, \tau, t), \rho(\varphi_2, \tau, t))$$

after uniform adjustment becomes:

$$\rho'(\varphi_1 \wedge \varphi_2, \tau, t) = \min(\rho(\varphi_1, \tau, t) - \delta, \rho(\varphi_2, \tau, t) - \delta)$$

Since $\min(a - \delta, b - \delta) = \min(a, b) - \delta$, we have:

$$\rho'(\varphi_1 \wedge \varphi_2, \tau, t) = \rho(\varphi_1 \wedge \varphi_2, \tau, t) - \delta$$

Again, the robustness shifts linearly by δ .

To prove the property for the *Until* operator, we again start from its definition

$$\begin{aligned}\rho(\varphi_1 \mathbf{U}_{[a,b]} \varphi_2, \tau, t) &= \\ &\max_{t' \in [t+a, t+b]} \left(\min \left(\rho(\varphi_2, \tau, t'), \min_{t'' \in [t, t']} \rho(\varphi_1, \tau, t'') \right) \right)\end{aligned}$$

After uniform adjustment:

$$\begin{aligned}\rho'(\varphi_1 \mathbf{U}_{[a,b]} \varphi_2, \tau, t) &= \\ &\max_{t' \in [t+a, t+b]} \left(\min \left(\rho(\varphi_2, \tau, t') - \delta, \min_{t'' \in [t, t']} \rho(\varphi_1, \tau, t'') - \delta \right) \right)\end{aligned}$$

Simplifying using properties of max and min:

$$\rho'(\varphi_1 \mathbf{U}_{[a,b]} \varphi_2, \tau, t) = \rho(\varphi_1 \mathbf{U}_{[a,b]} \varphi_2, \tau, t) - \delta$$

Hence, the robustness again shifts linearly by δ .

Finally, the proof for *Eventually* and *Globally* comes naturally from their definitions and the properties of max and min.

This concludes the proof that for any formula φ , the uniform adjustment of thresholds by a constant δ consistently shifts linearly the robustness value $\rho(\varphi, \tau, t)$. \square

C.2 Pruning

A summary of the simplifications applied can be found in Table 6.

C.2.1 Logical simplifications. This simplification procedure applies structural equivalences to STL formulae. Double negation is eliminated via $\neg(\neg\varphi) \rightarrow \varphi$, while De Morgan laws transform $\neg(\varphi \wedge \psi)$ into $\neg\varphi \vee \neg\psi$ and $\neg(\varphi \vee \psi)$ into $\neg\varphi \wedge \neg\psi$. Redundant binary expressions are collapsed using $\varphi \wedge \varphi \rightarrow \varphi$ and $\varphi \vee \varphi \rightarrow \varphi$. The simplifier also reduces combinations like $\varphi \wedge (\varphi \vee \psi)$ and $\varphi \vee (\varphi \wedge \psi)$ to φ .

Temporal nesting is flattened. Considering I and J as two generic temporal intervals, $G_I(G_J(\varphi))$ becomes $G_{I+J}(\varphi)$, and similarly $F_I(F_J(\varphi)) \rightarrow F_{I+J}(\varphi)$. When both children of an until operator are equal, the formula $\varphi U_I \varphi$ simplifies to φ . This procedure does not depend on data and only rewrites formulae based on their syntactic structure.

Table 6. STL formulae simplifications

Logical simplifications		Data-aware simplifications	
Original	Simplified	Original	Simplified
$\neg(\neg\varphi)$	φ	$\neg\text{True}$	False
$\neg(x \leq c)$	$x > c$	$\neg\text{False}$	True
$\neg(\mathbf{F}_I(\varphi))$	$\mathbf{G}_I(\neg\varphi)$	$\text{True} \wedge \varphi$	φ
$\neg(\mathbf{G}_I(\varphi))$	$\mathbf{F}_I(\neg\varphi)$	$\text{False} \wedge \varphi$	False
$\neg(\varphi_1 \vee \varphi_2)$	$\neg\varphi_1 \wedge \neg\varphi_2$	$\text{True} \vee \varphi$	True
$\neg(\varphi_1 \wedge \varphi_2)$	$\neg\varphi_1 \vee \neg\varphi_2$	$\text{False} \vee \varphi$	φ
$\varphi \wedge \varphi$	φ	$\mathbf{G}_{[0,\infty)}(\text{True})$	True
$\varphi \vee \varphi$	φ	$\mathbf{G}_{[0,\infty)}(\text{False})$	False
$\varphi \wedge (\varphi \vee \psi)$	φ	$\mathbf{F}_{[0,\infty)}(\text{True})$	True
$\varphi \vee (\varphi \wedge \psi)$	φ	$\mathbf{F}_{[0,\infty)}(\text{False})$	False
$\varphi \wedge (\varphi \wedge \psi)$	$\varphi \wedge \psi$	$\varphi \mathbf{U}_{[0,b]} \text{True}$	φ
$\varphi \vee (\varphi \vee \psi)$	$\varphi \vee \psi$	$\varphi \mathbf{U}_{[a,b]} \text{True}, a \neq 0$	$\mathbf{G}_{[0,a]}\varphi$
$\mathbf{G}_I(\mathbf{G}_J(\varphi))$	$\mathbf{G}_{I+J}(\varphi)$	$\varphi \mathbf{U}_I \text{False}$	False
$\mathbf{F}_I(\mathbf{F}_J(\varphi))$	$\mathbf{F}_{I+J}(\varphi)$	$\text{True} \mathbf{U}_I \varphi$	$\mathbf{F}_I(\varphi)$
$\varphi \mathbf{U}_I \varphi$	φ	$\text{False} \mathbf{U}_I \varphi$	False

Algorithm 3 Postprocess formulae based on robustness separation

Require: Set of formulae Φ , target class \hat{y} , input trajectory \mathbf{x} , trajectories by class $\{\mathcal{T}_1, \dots, \mathcal{T}_{K-1}\}$

Ensure: Postprocessed formulae Φ'

```

 $\Phi' \leftarrow \emptyset$ 
for  $\varphi \in \Phi$  do
   $r_{\text{target}} \leftarrow \rho(\varphi, \mathbf{x})$ 
  for  $k = 0$  to  $K - 1$  do
    if  $c \neq \hat{y}$  then
       $\mathcal{R}_k \leftarrow [\rho(\varphi, \tau) \text{ for } \tau \in \mathcal{T}_c]$ 
    else
       $\mathcal{R}_k \leftarrow [r_{\text{target}}]$ 
    end if
  end for
   $\mathcal{R}_{\text{opp}} \leftarrow \bigcup_{k \neq \hat{y}} \mathcal{R}_k$ 
   $n_{<} \leftarrow \#\{r \in \mathcal{R}_{\text{opp}} \mid r < r_{\text{target}}\}$ 
   $n_{>} \leftarrow \#\{r \in \mathcal{R}_{\text{opp}} \mid r > r_{\text{target}}\}$ 
  if  $n_{>} > n_{<}$  then
     $\varphi \leftarrow \neg\varphi$ 
     $r_{\text{target}} \leftarrow -r_{\text{target}}$ 
     $\mathcal{R}_{\text{opp}} \leftarrow [-r \mid r \in \mathcal{R}_{\text{opp}}]$ 
  end if
   $r_{\text{closest}} \leftarrow \max\{r \in \mathcal{R}_{\text{opp}} \mid r < r_{\text{target}}\}$ 
   $s \leftarrow (r_{\text{target}} + r_{\text{closest}})/2$ 
   $\varphi' \leftarrow \text{RescaleThresholds}(\varphi, -s)$ 
  if  $\rho(\varphi', \mathbf{x}) < 0$  then
     $\varphi' \leftarrow \neg\varphi'$ 
  end if
  append  $\varphi'$  to  $\Phi'$ 
end for
return  $\Phi'$ 

```

C.2.2 Data-aware simplifications. This method uses the evaluation of atomic predicates over a trajectory set \mathcal{T} to simplify STL formulae contextually. Each atom $\pi(\mathbf{x})$ is evaluated across all considered trajectories and at all time steps. If the predicate holds (resp. fails) for all samples at a given t , it is marked as true (resp. false). Otherwise, it is marked as undefined at that time step.

Given this truth map, each subformula is recursively reduced. An atom that is uniformly true (resp. false) is replaced by \top (resp. \perp). Boolean simplification is then applied, collapsing expressions like $\top \wedge \varphi$ to φ and $\perp \vee \varphi$ to φ .

D Experimental setting

In this section, we provide a detailed account of the training procedures used to develop the model presented in this paper. This includes information on the datasets, data preprocessing steps, and hyperparameter settings. These details are intended to ensure the reproducibility of our results and to offer insights into the training processes that led to the model performances reported in the main text.

D.1 Datasets and preprocessing

We base our experiments on a subset of time series classification tasks from the University of East Anglia (UEA) Time Series Archive (Bagnall, Dau, et al. 2018). This benchmark suite comprises over 140 univariate and multivariate datasets spanning diverse domains, including sensor readings, motion capture, physiological signals, and spectrographic measurements. For computational feasibility, we consider the first ten datasets in alphabetical order from the archive, excluding *DuckDuckGeese* due to hardware constraints. All datasets are loaded and standardised (zero mean and unit variance per channel), and processed using the aeon Python library (Middlehurst, Ismail-Fawaz, et al. 2024), which ensures consistency with other state-of-the-art time series classification benchmarks (Bagnall, Flynn, et al. 2020; Ruiz et al. 2021).

As the datasets are multivariate, we perform a preprocessing step to remove uninformative or redundant input variables. In particular, we discard variables whose temporal traces are strongly correlated across the dataset. This is achieved by computing the Pearson correlation matrix over all variable pairs after flattening the time dimension. Pairs exceeding a correlation threshold of 0.9 are reduced by keeping only the more informative variable (based on average absolute magnitude). This dimensionality reduction step improves training efficiency and robustness without compromising semantic diversity in the inputs.

We adopt the standard train/test splits provided by the aeon archive, which are consistent with previous evaluation protocols in the literature. However, for hyperparameter tuning, an internal development split was used to better estimate generalisation performance.

Computing infrastructure. All experiments were executed on a DELL PowerEdge R7525 server equipped with dual AMD EPYC 7542 CPUs (32 cores each), 768 GB RAM, and two NVIDIA A100 GPUs. The GPU resources were partitioned, with each run typically using up to 10 GB of GPU memory, and at most 20 GB for the largest datasets. CPU memory usage ranged between 20 GB and 150 GB, with only two datasets requiring allocations above 50 GB. All computations were performed using mixed CPU–GPU execution within a controlled HPC environment to ensure reproducibility and efficient resource utilisation.

Key dependencies included CUDA (12.8.0), PyTorch (2.2.1) (Paszke et al. 2019), and GPU-accelerated libraries for data processing and machine learning. The software stack also incorporated scikit-learn (1.6.1) (Pedregosa et al. 2011) and NumPy (1.26.2) (Harris et al. 2020) for numerical and statistical operations. PuLP (3.1.1) (Mitchell et al. 2011) was used to solve the ILP for global explanation extraction. As mentioned, aeon (1.1.0) (Middlehurst, Ismail-Fawaz, et al. 2024) was used to handle the datasets.

D.2 Training details

All experiments were conducted using PyTorch with deterministic seed initialisation to ensure reproducibility. Each model was trained using the Adam optimiser with batch-wise updates and default momentum parameters. Weighted cross-entropy loss was used to account for class imbalance, where class weights were computed as the inverse frequency of each class within the training data. In addition to the standard loss, the final objective included regularisation terms to control the sharpness of the concept relevance distribution and the magnitude of the learned robustness threshold ϵ , as will be detailed later. Gradients were clipped within reasonable bounds, and concept relevance scale parameters were constrained during training to avoid numerical instability.

To better balance learning dynamics between the main model parameters and regularisation controllers, we define two parameter groups with distinct learning rates. The primary model parameters (e.g., weights, classification head, embeddings) are updated with a standard learning rate, while the specialised parameters governing regularisation dynamics, such as concept relevance collapse strength and ϵ stability, are assigned a learning rate an order of magnitude higher, ensuring faster adaptation of these auxiliary components without destabilising the main optimisation process. As mentioned, both groups are optimised jointly using the Adam optimiser, allowing for robust and adaptive gradient updates across all layers.

Early stopping was employed with a configurable patience criterion during tuning, monitoring validation loss every few epochs. If no improvement was observed for a given number of consecutive validation checks, training was halted and the best model checkpoint (based on validation loss) was restored.

For each dataset, training was conducted on the official training split as provided by the `aeon` implementation of the UEA archive.

D.2.1 Hyperparameter tuning. We employed a two-stage Bayesian optimisation strategy using the `Ax` framework (Olson et al. 2025) to efficiently explore the hyperparameter space. The search was performed on a dedicated fold distinct from those later used for official evaluation, following an 80/20/20 train/validation/test split. Initial exploration was carried out using Sobol sampling to ensure broad coverage of the search space, followed by Bayesian optimisation leveraging `qNoisyExpectedImprovement` for single-objective tuning (accuracy) and `qLogNParEGO` or `qNoisyExpectedHypervolumeImprovement` (Daulton et al. 2021) for multi-objective tuning (accuracy and local separability).

The search space spanned the number of layers (0–3), learning rate (10^{-5} – 10^{-1}), initial concept relevance scale (0.5–2.0), and hidden layer dimension (256, 512, 1024). Other hyperparameters were fixed based on preliminary analysis: batch size (32), activation function (GELU), dropout rate (0.1), explanation threshold $\gamma_t = 0.8$, and concept generation parameters ($t = 0.99$, 500 concepts per variable, with a minimum of 1000 total concepts).

The optimisation consisted of an initial phase of 8 Sobol trials followed by an extensive Bayesian refinement phase with early stopping based on validation performance. For the multi-objective setup, Pareto-optimal configurations were identified to balance predictive accuracy and local explanation quality. The final configuration was chosen according to test set performance in the tuning phase and subsequently evaluated on the official 10-fold splits, training three independent seeds per fold. Reported results correspond to averages across all folds and seeds.

D.2.2 Loss function. The overall loss combines standard classification loss with regularisation terms that promote concept relevance interpretability and well-behaved robustness normalisation. It is defined as:

$$\mathcal{L} = \underbrace{\text{CE}(\mathbf{z}, \mathbf{y}; \mathbf{w})}_{\text{classification loss}} + \underbrace{\lambda_T \cdot \sigma\left(-\frac{T}{t}\right)}_{\text{concept relevance sharpness penalty}} + \underbrace{\lambda_\varepsilon \cdot (e^\varepsilon + e^{-\varepsilon})}_{\text{trajectory robustness regularisation}}$$

where:

- $\text{CE}(\mathbf{z}, \mathbf{y}; \mathbf{w})$ is the weighted cross-entropy loss between the predicted logits $\mathbf{z} \in \mathbb{R}^K$ and one-hot encoded labels $\mathbf{y} \in \{0, 1\}^K$, with class weights \mathbf{w} ,
- T is the scaling parameter used in Equation 4,
- t is the concept relevance temperature,
- ε is the learnable trajectory robustness parameter (used in Equation 2),
- $\sigma(\cdot)$ is the sigmoid function,
- λ_T and λ_ε are trainable strengths for each regulariser.

The concept relevance sharpness term encourages concentrated distributions while avoiding instability through smooth sigmoid control. The robustness regulariser penalises extreme values of ε , promoting stable discriminability across concepts. Both regularisation terms are softly enforced via learnable scaling coefficients, allowing the model to dynamically balance interpretability and predictive performance during training.

Reproducibility Checklist for JAIR

Select the answers that apply to your research – one per item.

All articles:

- (1) All claims investigated in this work are clearly stated. [yes/partially/no] Yes
- (2) Clear explanations are given how the work reported substantiates the claims. [yes/partially/no] Yes
- (3) Limitations or technical assumptions are stated clearly and explicitly. [yes/partially/no] Yes
- (4) Conceptual outlines and/or pseudo-code descriptions of the AI methods introduced in this work are provided, and important implementation details are discussed. [yes/partially/no/NA] Yes
- (5) Motivation is provided for all design choices, including algorithms, implementation choices, parameters, data sets and experimental protocols beyond metrics. [yes/partially/no] Partially

Articles containing theoretical contributions:

Does this paper make theoretical contributions? [yes/no] Yes

If yes, please complete the list below.

- (1) All assumptions and restrictions are stated clearly and formally. [yes/partially/no] Yes
- (2) All novel claims are stated formally (e.g., in theorem statements). [yes/partially/no] Yes
- (3) Proofs of all non-trivial claims are provided in sufficient detail to permit verification by readers with a reasonable degree of expertise (e.g., that expected from a PhD candidate in the same area of AI). [yes/partially/no] Yes
- (4) Complex formalism, such as definitions or proofs, is motivated and explained clearly. [yes/partially/no] Yes
- (5) The use of mathematical notation and formalism serves the purpose of enhancing clarity and precision; gratuitous use of mathematical formalism (i.e., use that does not enhance clarity or precision) is avoided. [yes/partially/no] Yes
- (6) Appropriate citations are given for all non-trivial theoretical tools and techniques. [yes/partially/no] Yes

Articles reporting on computational experiments:

Does this paper include computational experiments? [yes/no] Yes

If yes, please complete the list below.

- (1) All source code required for conducting experiments is included in an online appendix or will be made publicly available upon publication of the paper. The online appendix follows best practices for source code readability and documentation as well as for long-term accessibility. [yes/partially/no] Yes
- (2) The source code comes with a license that allows free usage for reproducibility purposes. [yes/partially/no] Yes
- (3) The source code comes with a license that allows free usage for research purposes in general. [yes/partially/no] Yes
- (4) Raw, unaggregated data from all experiments is included in an online appendix or will be made publicly available upon publication of the paper. The online appendix follows best practices for long-term accessibility. [yes/partially/no] Yes
- (5) The unaggregated data comes with a license that allows free usage for reproducibility purposes. [yes/partially/no] Yes
- (6) The unaggregated data comes with a license that allows free usage for research purposes in general. [yes/partially/no] Yes
- (7) If an algorithm depends on randomness, then the method used for generating random numbers and for setting seeds is described in a way sufficient to allow replication of results. [yes/partially/no/NA] Yes

- (8) The execution environment for experiments, the computing infrastructure (hardware and software) used for running them, is described, including GPU/CPU makes and models; amount of memory (cache and RAM); make and version of operating system; names and versions of relevant software libraries and frameworks. [yes/partially/no] Yes
- (9) The evaluation metrics used in experiments are clearly explained and their choice is explicitly motivated. [yes/partially/no] Yes
- (10) The number of algorithm runs used to compute each result is reported. [yes/no] Yes
- (11) Reported results have not been “cherry-picked” by silently ignoring unsuccessful or unsatisfactory experiments. [yes/partially/no] Yes
- (12) Analysis of results goes beyond single-dimensional summaries of performance (e.g., average, median) to include measures of variation, confidence, or other distributional information. [yes/no] Yes
- (13) All (hyper-) parameter settings for the algorithms/methods used in experiments have been reported, along with the rationale or method for determining them. [yes/partially/no/NA] Yes
- (14) The number and range of (hyper-) parameter settings explored prior to conducting final experiments have been indicated, along with the effort spent on (hyper-) parameter optimisation. [yes/partially/no/NA] Yes
- (15) Appropriately chosen statistical hypothesis tests are used to establish statistical significance in the presence of noise effects. [yes/partially/no/NA] Yes

Articles using data sets:

Does this work rely on one or more data sets (possibly obtained from a benchmark generator or similar software artifact)? [yes/no] Yes

If yes, please complete the list below.

- (1) All newly introduced data sets are included in an online appendix or will be made publicly available upon publication of the paper. The online appendix follows best practices for long-term accessibility with a license that allows free usage for research purposes. [yes/partially/no/NA] NA
- (2) The newly introduced data set comes with a license that allows free usage for reproducibility purposes. [yes/partially/no] NA
- (3) The newly introduced data set comes with a license that allows free usage for research purposes in general. [yes/partially/no] NA
- (4) All data sets drawn from the literature or other public sources (potentially including authors' own previously published work) are accompanied by appropriate citations. [yes/no/NA] Yes
- (5) All data sets drawn from the existing literature (potentially including authors' own previously published work) are publicly available. [yes/partially/no/NA] Yes
- (6) All new data sets and data sets that are not publicly available are described in detail, including relevant statistics, the data collection process and annotation process if relevant. [yes/partially/no/NA] NA
- (7) All methods used for preprocessing, augmenting, batching or splitting data sets (e.g., in the context of hold-out or cross-validation) are described in detail. [yes/partially/no/NA] Yes

Explanations on any of the answers above (optional):

Regarding questions (2) and (3) of the "articles using data sets": we did not introduce any new dataset

Received October 2025